Opportunities from Doping of Non-Critical Metal Oxides in Last Generation Light-Conversion Devices

ADVANCED ENERGY MATERIALS
www.advenergymat.de

Opportunities from Doping of Non-Critical Metal Oxides in Last Generation Light-Conversion Devices

Teresa Gatti, Francesco Lamberti,* Raffaello Mazzaro, Ilka Kriegel, Derck Schlettwein, Francesco Enrichi, Nicolò Lago, Eleonora Di Maria, Gaudenzio Meneghesso, Alberto Vomiero, and Silvia Gross**

The need to develop sustainable energy solutions is an urgent requirement for society, with the additional requirement to limit dependence on critical raw materials, within a virtuous circular economy model. In this framework, it is essential to identify new avenues for light-conversion into clean energy and fuels exploiting largely available materials and green production methods. Metal oxide semiconductors (MOSs) emerge among other species for their remarkable environmental stability, chemical tunability, and optoelectronic properties. MOSs are often key constituents in next generation energy devices, mainly in the role of charge selective layers. Their use as light harvesters is hitherto rather limited, but progressively emerging. One of the key strategies to boost their properties involves doping, that can improve charge mobility, light absorption and tune band structures to maximize charge separation at heterojunctions. In this review, effective methods to dope MOSs and to exploit the derived benefits in relation to performance enhancement in different types of devices are identified and critically compared. The work is focused specifically on the best opportunities coming from the use of non-critical raw materials, so as to contribute in defining an economically feasible roadmap for light conversion technologies based on these highly stable and widely available compounds.

1. Introduction

The materials science community is required to contribute consistently to a paradigm-change within existing productive models, by proposing new platforms for a sustainable "materials economy" that paves the way to commercial products of large availability (supply issue), long-term duration (life cycle issue), good perspectives for complete reuse (recycling issue) and complying also with economic sustainability (cost issue). Renewable energy technologies are at the forefront of a worldwide effort to limit the dependence on fossil fuels and to reduce the impact of greenhouse gases emission on climate change. In this context, most key players at the global level have defined roadmaps to reach these goals. The European Union (EU), has defined a growth strategy (the "European Green Deal") that points at a carbon-neutral Europe by 2050 while implementing a circular economy model

Dr. T. Gatti, D. Schlettwein
Center for Materials Research
Justus Liebig University Giessen
Heinrich Buff Ring 17, 35392 Giessen, Germany
E-mail: teresa.gatti@phys.chemie.uni-giessen.de
Dr. F. Lamberti, Prof. S. Gross
Department of Chemical Sciences
University of Padova
via Marzolo 1, Padova 35131, Italy
E-mail: francesco.lamberti@unipd.it; silvia.gross@unipd.it
Dr. F. Lamberti, Prof. E. Di Maria, Prof. G. Meneghesso, Prof. S. Gross
Interdepartmental Centre Giorgio Levi Cases for Energy Economics and Technology
University of Padova
via Marzolo 9, Padova 35131, Italy

The ORCID identification number(s) for the author(s) of this article can be found under https://doi.org/10.1002/aenm.202101041.

DOI: 10.1002/aenm.202101041

Dr. R. Mazzaro
Institute for Microelectronics and Microsystems
Italian National Research Council
Section of Bologna, Bologna 40129, Italy
Dr. I. Kriegel
Functional Nanosystems
Italian Institute of Technology
via Morego 30, Genova 16163, Italy
Dr. F. Enrichi
CNR-ISP
Institute of Polar Sciences
National Research Council
Via Torino 155, Mestre-Venezia 30172, Italy
Dr. F. Enrichi, Prof. A. Vomiero
Department of Molecular Sciences and Nanosystems
Ca' Foscari University of Venice
via Torino 155, Venezia 30172, Italy
Dr. N. Lago, Prof. G. Meneghesso
Department of Information Engineering
University of Padova
Via Gradenigo 6/B, Padova 35131, Italy
Prof. E. Di Maria
Department of Economics and Management "Marco Fanno"
University of Padova
Via del Santo 33, Padova 35123, Italy

that aims at an efficient use of resources and at optimized manufacturing processes.[1] The realization of these ambitious goals cannot disregard a critical assessment on the availability of raw materials are the building blocks of most key enabling technologies.[2] Critical raw materials (CRMs) are indeed under continuous monitoring of the European Commission (EC) since 2011, with a list that is updated almost every year with new entries and guidelines employed to identify them (the last update in 2020 include 30 critical raw materials and outlines their importance for strategic technologies such as batteries, photovoltaics (PV), wind energy, fuel cells, robotics, and others).[3–5] As a consequence, in Europe (and worldwide) there is a burgeoning need to pinpoint "substitute materials" for current technologies, being these already present on the market or still under development in research laboratories.

In this perspective, we set the focus on existing and emerging technological concepts for solar energy conversion (i.e., PV, photoelectrochemical methods for the production of solar fuels, photon up and down conversion, photocapacitors, and others), being these essential pillars of a future sustainable society fueled by clean energy sources. We also identify metal oxide semiconductors (MOSs) as a class of materials which has great potential to constitute the basis for the further development of these technologies into actual models of "low-criticality" for our economy.[6] MOSs are indeed characterized by a considerable stability to typical environmental factors, ease of synthesis and processing and already act as essential building blocks in other established and/or emerging technologies, such as batteries,[7,8] superconductors,[9] thermoelectrics and piezoelectrics,[10,11] fuel cells,[12] smart windows,[13] and the more recent quantum technologies.[14,15] Their intrinsic optoelectronic properties can be boosted by employing doping strategies and, for this reason, we further shift the focus on this particular aspect and the opportunities emerging from their informed doping strategies.

For some of the indicated strategic technologies, a detailed analysis on the availability of resources has been carried out in 2020 by the EC.[5] As presently dominating technology of solar energy conversion, silicon PV is mainly based on elements with a low supply risk. However, the production of cells requires a high input of energy, which by today´s mix leads to high emission of CO_2.[16] New PV technologies aiming at lower energy payback time are, therefore, looked for.[17] In order to provide valuable guidelines on the application of MOSs in this context it is essential to examine and establish options of using those MOSs that are based on earth abundant and non-CRMs. From the diagram reproduced in **Figure 1**a,[5] it emerges how some metals such as those belonging to the group of the rare earth elements as well as cobalt, with interesting properties for use in light conversion, are characterized by very high to moderate risk of supply, while others with as much relevance for this field like titanium, tungsten, copper, and nickel are listed among those with low to very low criticality or, like iron, for which no supply risk is seen.

Such analysis highlights how the risk of potential bottlenecks in the supply of raw materials is related to a growth of demand in terms of quantity (rates in the increase of areas of applications, i.e., renewables vs defense and space) as well as to other variables (geopolitical situation, costs of mining/extracting, and processing/refining). High rates of growth of the demand for specific raw materials may increase their prices, thus becoming an opportunity for companies to invest in risky geographical areas or in more expensive technologies not affordable before. Moreover, a still limited supply from secondary sources (recycled from waste) arising from a still underdeveloped circularly economy framework[18] reduces alternative options of supply, thus posing attention on the actual and dynamic supply chain for CRMs. The limited internal stock of resources at the EU level (**Figure 2**) push companies in EU to rely on external supply, where China is the main country contributing as the largest shares of EU import of CRMs (**Table 1** and **Figure 3**), followed by USA, Russia, and Mexico. At the international level, particular attention is given to the social sustainability of the supply chain of CRMs (responsible supply chain)[19] and the potential consequences in terms of supply risks. In addition to costs connected to the activity of mining/extracting and processing/refining, it becomes also important to develop a responsible supply chain that takes into account the enforcement of human rights and avoids contributions to conflicts through their mineral purchasing decisions and practice. From this point of view the environmental and social perspectives are coupled in the definition of strategic directions for the identification of CRMs (environmental availability and social desirability/feasibility).[20] In 2014, the European Commission released a new legislation (Regulation (EU 2017/821), active from 1 January 2021), to ensure that European companies will in future trade minerals responsibly and aimed at promoting companies transparency and encouraging them to adopt a more sustainable approach to sourcing.

According to the Organization for Economic Cooperation and Development (OECD),[21] despite improvements in materials intensity and resource efficiency, there will be an increase in the global material use by 2060, that specifically for metals will lead to a +150% (from 8 to 20 billion tons). In this scenario, EU is depending on imports of more than 75% of the required materials.

The EU Raw Material Scoreboard[23] confirms the overall dependence of the EU from import of raw materials, but also the associated risks connected to control (governance level) of the supply. Relevant differences are revealed in terms of the country mix between global production and supply to the EU, where high levels of dependence from import such as in the case of heavy rare earth elements (HREE) and light rare earth elements (LREE) is combined with different risks of more abundant materials produced domestically at the EU level. Up to now, the cost of production for metals at the EU level (mining exploration and extraction) as well as the limited contribution related to the recycling processes within the circular economy approach has limited the EU autonomy in materials production. The EU remains a producer of several basic metals (i.e., copper, lead, iron ore) The EU also has mines of several critical raw materials (i.e.,

Prof. A. Vomiero
Division of Materials Science
Department of Engineering Sciences and Mathematics
Luleå University of Technology
Luleå 97187, Sweden
Prof. S. Gross
Karlsruher Institut für Technologie (KIT)
Institut für Technische Chemie und Polymerchemie (ITCP)
Engesserstr. 20, 76131 Karlsruhe, Germany

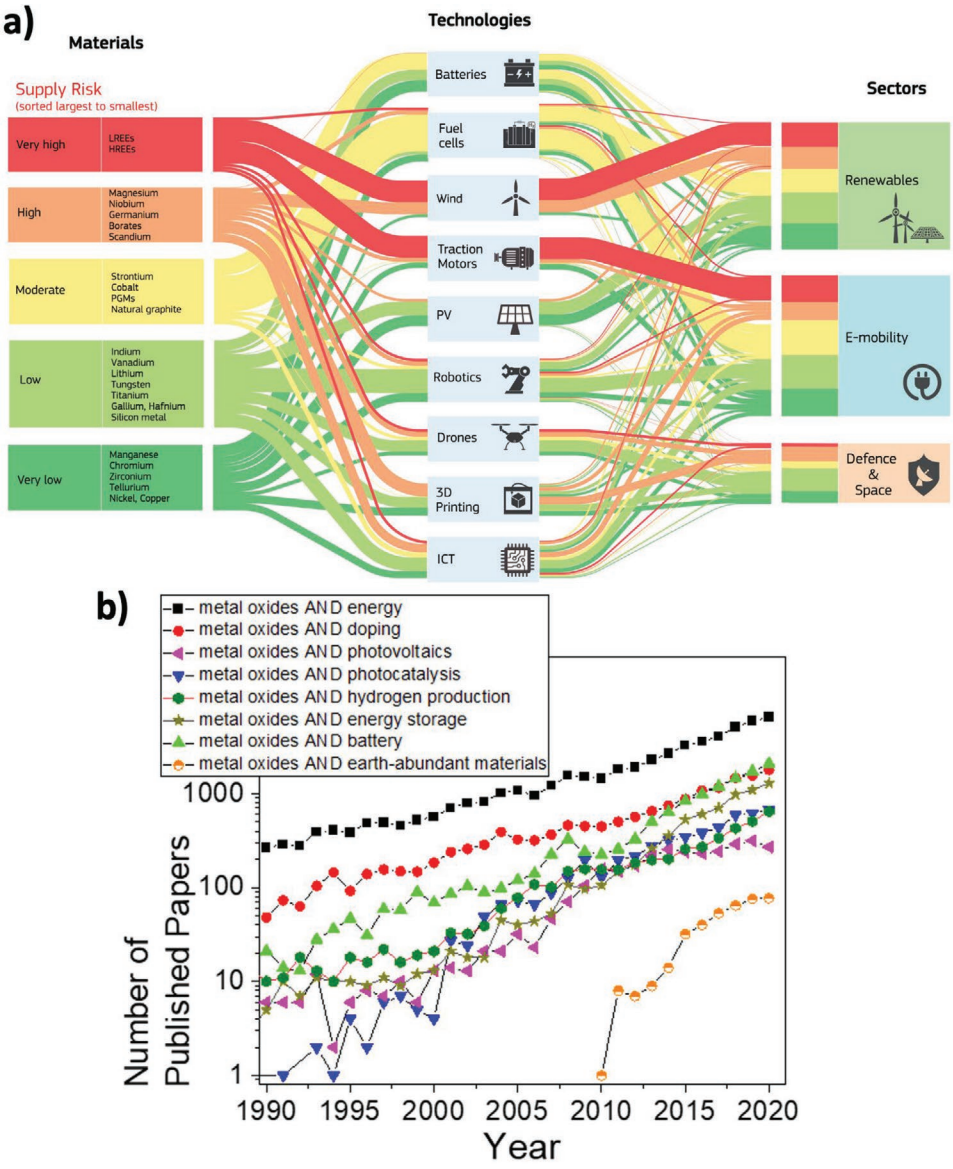

Figure 1. a) Diagram depicting the supply risks assigned to several CRMs of large use in essential technologies. Reproduced with permission.[5] Copyright 2020, European Union. b) Trends in published scientific papers (until December 2020, source: Scopus) dealing with the use of metal oxides in different contexts. The exact keywords used for the different searches are reported in the caption. A logarithmic scale is applied on the ordinate axis given the high numbers involved.

graphite, tungsten, phosphate, and vanadium), which are mainly concentrated in Finland, Sweden, and Spain, and some potential sites for rare earth element (REE) mining.[24] Nevertheless, despite continuous investments in this direction by expansion of mining activity and domestic production of metals, which highlights the strategic attention to the problem, the related domestic production is currently not sufficient to satisfy the demand for raw materials, and import reliance remains high.

We thus maintain as leitmotif in the following discussion the intention to provide a critical assessment on the opportunities deriving from the use of the most earth-abundant MOSs in this type of applications, even if these particular species might not be champions of efficiency in a given technology. This is of course an arguable choice, as it is also true that a material platform, even if extremely critical in its supply, can be still highly economically valuable and even contribute to a more sustainable society if it is capable of ensuring the best and longest-lasting performance achievable in that sector. Nonetheless, we decided to adopt the aforementioned point of view in this perspective in order to provide a strategy that is based on recent scientific progress but also takes into account the boundary conditions provided by the political and economic framework in which present developments of new technologies occur.

The high current impact of MOSs in energy-related applications and, particularly, in those connected to light-conversion, is shown in Figure 1b. The graph shows the trend in published papers reporting on the more general keyword “metal oxide” and “energy” exponentially (the scale is logarithmic) growing over the

Figure 2. EU production of primary CRMs in tons (and share of supply to EU from 2010 to 2014). Adapted under the terms of the CC-BY license.[18,22] Copyright 2018, 2020, European Commission.

last 30 years. Interestingly, the same trend is found when combining the first keyword with "doping": it seems reasonable to state that the research on doping somehow has been and will be able to sustain the research on new MOSs applications in the field of energy, motivating the focus of the present perspective on this particular aspect to search for the best future opportunities for this class of materials. On the other hand, the interest in the use of MOSs in light-conversion applications, such as those exemplified here by the keywords "photovoltaics" and "photocatalysis" (and partially also by "hydrogen production") show a more moderate growth over the analyzed period. A reason for this, particularly for the case of PV, might be caused by competition with other materials as rising stars of this technology, namely metal halide perovskites. Nevertheless, we believe that a shift in paradigm toward MOSs could offer new opportunities for the development of low-cost devices with attractive energy payback time and an improved stability when compared to devices based on perovskites, which up to now are still suffering enormously from this drawback.[25,26] Furthermore, it should also be considered that MOSs are key materials to ensure proper functioning of perovskite solar cells (PSCs):[27] MOSs are often the main constituents of ancillary layers such as the electron and hole transporting layers (also in organic PV[28]) and thus, even if they are not often featured within keywords, they still play a major role in device development (some considerations on this use of MOSs will appear in a later paragraph). From the graph in Figure 1b, we can further notice that the impact of MOSs is perhaps more pronounced in the field of energy storage (with the exact keywords "battery" and "energy storage" here employed for the search), with a notable growth over the last 15 years, most likely guided by the search for well-performing all-solid-state batteries and supercapacitors.[7,29,30] The use of MOSs in these technologies inspired the present perspective toward application of non-CRMs-based devices in light-conversion. It is reasonable to believe that a future entrance in the market of MOSs-based light-conversion devices could be facilitated by their development in close contact with that of the sister technologies in energy storage. Finally, we also inserted a specific search including the keyword "earth-abundant materials" to test if the field is already established or still at its initial stage. As it can be seen, the topic, in specific reference to MOSs, appears to be yet under-investigated and started to emerge only a decade ago, with a very low number of

Table 1. Selected critical raw materials: main global producers and main EU sourcing countries.[21]

Raw materials	Stage	Main global producers	Main EU sourcing[a] countries
Antimony	Extraction	China (74%) Tajikistan (8%) Russia (4%)	Turkey (62%) Bolivia (20%) Guatemala (7%)
Baryte	Extraction	China (38%) India (12%) Morocco (10%)	China (38%) Morocco (28%) Other EU (15%) Germany (10%) Norway (1%)
Bauxite	Extraction	Australia (28%) China (20%) Brazil (13%)	Guinea (64%) Greece (12%) Brazil (10%) France (1%)
Beryllium	Extraction	United States (88%) China (8%) Madagascar (2%)	n/a
Bismuth	Processing	China (85%) Lao Pdr (7%) Mexico (4%)	China (93%)
Borate	Extraction	Turkey (42%) United States (24%) Chile (11%)	Turkey (98%)
Cobalt	Extraction	Congo DR (59%) China (7%) Canada (5%)	Congo DR (68%) Finland (14%) French Guiana (5%)
Coking coal	Extraction	China (55%) Australia (16%) Russia (7%)	Australia (24%) Poland (23%) United States (21%) Czechia (8%) Germany (8%)
Fluorspar	Extraction	China (65%) Mexico (15%) Mongolia (5%)	Mexico (25%) Spain (14%) South Africa (12%) Bulgaria (10%) Germany (6%)
Gallium	Processing	China (80%) Germany (8%) Ukraine (5%)	Germany (35%) UK (28%) China (27%) Hungary (2%)
Germanium	Processing	China (80%) Finland (10%) Russia (5%)	Finland (51%) China (17%) UK (11%)
Hafnium	Processing	France (49%) United States (44%) Russia (3%)	France (84%) United States (5%) UK (4%)
Indium	Processing	China (48%) Korea, Rep. (21%) Japan (8%)	France (28%) Belgium (23%) UK (12%) Germany (10%) Italy (5%)
Lithium	Processing	Chile (44%) China (39%) Argentina (13%)	Chile (78%) United States (8%) Russia (4%)
Magnesium	Processing	China (89%) United States (4%)	China (93%)
Natural Graphite	Extraction	China (69%) India (12%) Brazil (8%)	China (47%) Brazil (12%) Norway (8%) Romania (2%)
Natural Rubber	Extraction	Thailand (33%) Indonesia (24%) Vietnam (7%)	Indonesia (31%) Thailand (18%) Malaysia (16%)
Niobium	Processing	Brazil (92%) Canada (8%)	Brazil (85%) Canada (13%)
Phosphate rock	Extraction	China (48%) Morocco (11%) United States (10%)	Morocco (24%) Russia (20%) Finland (16%)
Phosphorus	Processing	China (74%) Kazakhstan (9%) Vietnam (9%)	Kazakhstan (71%) Vietnam (18%) China (9%)
Scandium	Processing	China (66%) Russia (26%) Ukraine (7%)	UK (98%) Russia (1%)
Silicon metal	Processing	China (66%) United States (8%) Norway (6%) France (4%)	Norway (30%) France (20%) China (11%) Germany (6%) Spain (6%)
Strontium	Extraction	Spain (31%) Iran, Islamic Rep. (30%) China (19%)	Spain (100%)
Tantalum	Extraction	Congo, DR (33%) Rwanda (28%) Brazil (9%)	Congo, DR (36%) Rwanda (30%) Brazil (13%)
Titanium[b]	Processing	China (45%) Russia (22%) Japan (22%)	n/a
Tungsten[c]	Processing	China (69%) Vietnam (7%) United States (6%) Austria (1%) Germany (1%)	n/a
Vanadium[d]	Processing	China (55%) South Africa (22%) Russia (19%)	n/a
Platinum Group Metals[e]	Processing	South Africa (84%) - iridium, platinum, rhodium, ruthenium Russia (40%) - palladium	n/a
Heavy Rare Earth Elements[f]	Processing	China (86%) Australia (6%) United States (2%)	China (98%) Other non-EU (1%) UK (1%)
Light Rare Earth Elements	Processing	China (86%) Australia (6%) United States (2%)	China (99%) UK (1%)

[a]Based on Domestic production and Import (Export excluded); [b]For Titanium metal sponge there are no trade codes available for the EU; [c]The distribution of tungsten smelters and refiners has been used as a proxy of the production concentration. Trade data are not completely available for commercial confidentiality reason; [d]The EU import reliance cannot be calculated for the vanadium, as there is no production and trade for vanadium ores and concentrates in the EU; [e]The trade data include metal from all sources, both primary and secondary. It was not possible to identify the source and the relative contributions of primary and secondary materials; [f]Global production refers to Rare Earth Oxides concentrates for both Light and Heavy Rare Earth Elements.

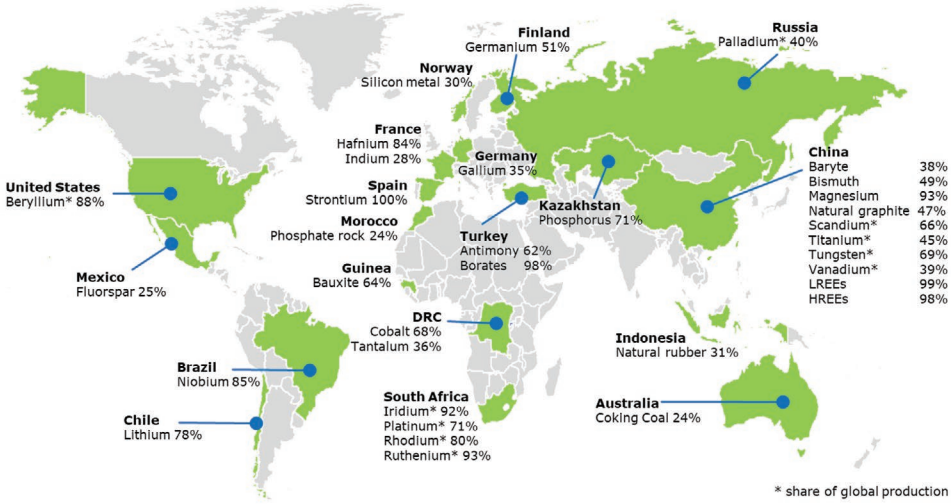

Figure 3. Countries accounting for largest share of global supply of CRMs. Adapted under the terms of the CC-BY license.[22] Copyright 2020, European Commission.

contributions addressing it, but with a relatively pronounced factor of tenfold increase in the number of annually published papers within ten years. With this contribution, we hope to encourage and give momentum to presently ongoing and future research on earth-abundant MOSs for use in energy technologies, in particular allowing the conversion of solar light into other forms of energy, directly contributing to a sustainable development.

In Section 2, we will address the particular aspect related to the rational design of MOS doping strategies, trying to define guidelines that answer the general question: which dopant should be chosen for a given (preferably earth-abundant) MOS to improve its properties toward more efficient light-conversion? In addition, the most effective analytical methods useful to characterize dopants within a MOSs structure (amount and arrangement in the lattice, concomitant defects introduced) will be discussed, to overcome the lack of detailed structural information that is sometimes found in reports on doped MOSs. It is certainly of the utmost importance to analyze the structure of these species to be able to address the design of further improved materials. Section 3 will examine specific cases of non-critical doped MOSs in light-conversion technologies as possible substitutes for current champions based on CRMs: the number of examples in this direction is still rather limited, but the species discussed here undoubtedly represent the starting point for future developments of the field in directions of pronounced sustainability.

2. Doping of MOSs

2.1. Theoretical Background and Design Strategies for the Rationale Doping of MOSs Active in Light-Conversion

Chemically, oxides are compounds in which at least one element is oxygen with the oxidation state -II (O^{2-}). For the purposes if this perspective, we focus on crystalline solid metal oxides (MOs). The 3D packaging becomes fundamental for determining the properties of the materials. In detail, rutile, rock-salt, spinel, and perovskite structures are three of the most common lattice types, derived from closed-packed lattices: rutile (TiO_2, NbO_2, RuO_2) is a MO_2 structure in which the cations are octahedrally coordinated by anions in a 6:3 ratio;[31] rock-salt (like MgO, NiO, or CoO) are face-centered cubic (FCC) crystals with one metal ion surrounded by 6 nearest neighbors oxygen ions and vice versa.[32] Spinels (AB_2O_4, like ferrites or Co_3O_4[33]) and perovskite/double perovskites (ABO_3/$A'A''B_2O_6$ like $LaTiO_3$, Bi_2FeCrO_6) are ternary (or even quaternary) oxides in which A and B ions are tetrahedrally and octahedrally coordinated cations in the former, also depending on the inversion degree, whereas for the latter, a cubic FCC symmetry is present, where B-site cations fill ¼ of the octahedral vacancies surrounded by six oxide anions. Spinels and perovskites are of particular interests for their magnetic and ferroelectric properties due to the possibility of creating spontaneous polarization caused by distortion of the octahedra,[34] peculiar properties that can be notably improved when impurities are inserted in the structures, i.e., a chemical doping is introduced.[35,36]

Doping and defects are roughly correlated when discussing on semiconducting properties in MOSs. Heteroatoms in a lattice can be considered as defects for the hosting lattice structure, so that the related chemistry and theoretical aspects can be treated accordingly. The exact knowledge on the thermodynamics of dopants/defects provides a comprehensive understanding of such complex systems. The chemical bond in metal oxides is in many cases ionic: this feature allows to straightforwardly calculate the lattice energy of an ionic solid and to derive the electron affinities for oxygen (ΔE)[37]

$$O + e^- \rightarrow O^- \ (\Delta E = -1.46\ \text{eV}) \quad (1)$$

$$O^- + e^- \rightarrow O^{2-} \ (\Delta E > 0\ \text{eV}) \quad (2)$$

This result reveals a $2p^6$ configuration of oxygen in the solids, achieving a stable diamagnetic arrangement, strongly related to atmospheric oxygen that affects the electronic properties of MOSs.

The Madelung potential[38–40] can serve as a measure for the structural diversity of MOs and it is correlated to the lattice

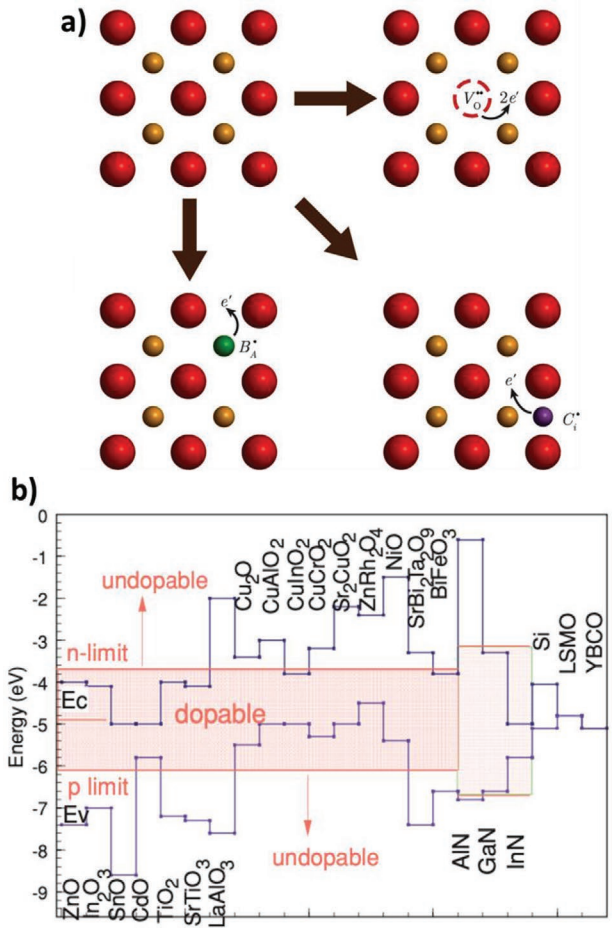

Figure 4. a) Schematics of charged defects identities in doped MOSs. Reproduced with permission.[41] Copyright 2014, American Chemical Society. b) Valence and conduction band energies of various MOSs versus vacuum level, with the doping limits showing the dopable and undopable cases. Reproduced with permission.[52] Copyright 2011, American Physical Society.

energy. Therefore, before critically reviewing recent advances it is noteworthy to understand the role of oxygen in these particular solids. In addition, conduction bands in MOSs are generally constituted of contributions from orbitals of the metal cations, while the valence bands feature major contributions by oxygen 2p orbitals.

The Madelung constant, being conceived for the bulk, can be also used for explaining the surface defect behavior of MOs: however some discrepancies occur when studying the ionization energies and energy gaps by considering the correlation between formal oxidation of the metal and the electrostatic environment of the oxide anion:[37] a more sophisticated model including long-range polarization employing explicit electronic structure techniques is required.

Transition metal cations, due to their partially filled *d* and even totally filled *f* orbitals, can easily change their valence state depending on temperature and oxygen partial pressure. A metal deficiency results in cation vacancies, whereas excess metal atoms are accommodated as interstitial cations. On the other hand, oxygen vacancies can be present. The thermodynamics of the lattice requires the system as a whole to be neutral and for this reason an acceptor or donor impurity (i.e., with lower or higher charge) is included. In such a way, oxygen vacancies are formed when positively charge defects are present, or electrons or cations vacancies emerge when a donor cation is incorporated (**Figure 4**a).[41] In such a way, oxygen vacancies are formed when positively charged defects are present, or electrons or cations vacancies emerge when a donor cation is incorporated (Figure 4a).[42] The role of point defects in different MOSs has been also reviewed.[43–46] Particular attention should be given to oxygen vacancies, which are of fundamental relevance in applications, in which the reactivity of the defective surface is important (for example catalysis), but also in those of optoelectronics.[47] Intrinsic doping resulting from native point defects has been recognized playing a critical role in defining most of the optoelectronic properties of ZnO,[48] NiO,[49] and Fe_2O_3.[50] Oxygen vacancies have magnetic characteristics that can be studied by magnetic spectroscopic techniques (mostly electron paramagnetic resonance, EPR) for understanding the carrier concentration in MOSs.[51] The properties of doped MOSs critically depend on excess oxygen or oxygen deficiency. In this way, e.g., charged impurity centers are compensated by lattice defects. Furthermore, it has been proven that the formation energy of the native defects can alter the Fermi level of the metal oxide, thus limiting the effective doping ability as highlighted in Figure 4b for some common MOSs.[52] For this reason, applications that involve charge transport are most heavily influenced by point defects: one of this applications is therefore the photovoltaics.

The PV effect is based on the possibility to create electron–hole-pairs within a light absorber: the larger the distance between the two photocharges, the higher is the possibility to suppress their recombination and to harvest them to an external circuit for producing a current. In order for this to happen efficiently, several ancillary layers are needed. MOSs are mostly used in this field because the presence of native defects in their structures or externally added impurities (dopants) support such extraction of the photo-induced charges,[53] positively affecting the overall efficiency of the solar cell. However, although the resulting effect is similar to the well-known boron or phosphorous doping in crystalline silicon, where the "extra" charge is used for achieving conductivity at RT, here the amount of guest species is much higher than in doped silicon: in fact, in the case of silicon electronics, the doping concentration is of the order of 10^{-2} at%, whereas for typical chemical doping concentration of heteroatoms in MOSs is of the order of 1–10 at%, i.e., 100–1000 times higher, thus providing quite different (and often) unpredictable properties. This aim for MOSs in PV to favor transport/extraction of charges across the different layers by avoiding carrier recombination is often achieved by fine-tuning the Fermi level within the MOSs, typically by transition metal impurities.

One important parameter to discuss the choice of chemical dopants consists in tolerance factors, i.e., a quantitie that correlates the ionic radii of the different ions constituting the lattice. The most famous one is the Goldschmidt tolerance factor, *t*:[54]

$$t = \frac{r_A + r_B}{\sqrt{2}(r_B + r_X)} \quad (3)$$

where r_i represents the ionic radius of the different ions A, B, X (X = O^{2-} but also halide) of the perovskite structure with the generic chemical formula ABX_3. The tolerance factor has

obtained great appreciation in these last years because of the huge impact of halide perovskites research in photovoltaics rapidly developing toward devices aiming at the performances of single crystal silicon devices (29.5% efficiency[55]): a lot of papers focusses on the effects of doping halide perovskites, opening the way to applications of these intriguing materials also in other fields beyond solar technology.[56] For this reason, new quantities are emerging for better predicting the structural stability of perovskites, taking into account the oxidation states of cations[57] also in the case of double perovskites ($A_2BB'X_6$), an interesting class of materials already well studied,[58,59] or the use of 3D constraints like the octahedral factor[60] in particular for perovskite oxides (ABO_3 structures).

For what concerns the energetics of the MOSs, the presence of donor/acceptor impurities produces the band-bending of the bands caused by up- or down-shifting of the Fermi level. Many phenomena such as electron or hole capture, electron or hole emission, hole and electron capture by a recombination center in a trap-assisted event, scattering of a charge carrier near a point defect, etc., directly depend on the presence of dopants. Dopants lead to favorable or unfavorable alignment of the ancillary layers and strongly affect the overall device performance.[61] Spectroscopic insights (ultrafast[62] and magnetic-based ones mainly) and modeling[63] are required for understanding the characteristics of these traps, being shallow or deep, in MOSs, which are often wide band gap materials like TiO_2, ZnO, or SnO_2.

From a microscopic point of view, at low applied electric fields, charge transport in MOSs is given by small polarons that tunnel to the next available free site following Mott's variable-range hopping (VRH) model for disordered materials.[64,65] In agreement with the VRH theory, the conductivity in MOSs and other disordered materials is given by (4)

$$\sigma(T) = \sigma_0 \cdot \exp\left\{-\left(\frac{18}{g(E_F)\cdot k_B T \cdot a^3}\right)^{\frac{1}{4}}\right\} \quad (4)$$

With a the localization radius of states, and $g(E_F)$ the density of states (DOS) at the Fermi level E_F, where $g(E)$ is typically assumed to have an exponential shape $g(E) = N_0 \exp(-E/E_T)$.

The above equation shows that

$$\ln(\sigma) \approx \left(\frac{1}{g(E_F)\cdot T}\right)^{\frac{1}{4}} \quad (5)$$

Therefore, measurements of the sample resistance performed at various temperatures allows to draw an Arrhenius plot ($\ln(\sigma)$ vs 1/T) that, in this particular case, leads to a direct estimate of the DOS near the given Fermi level[64,66] and to investigate how doping impacts on the transport properties of the material as well as its energy levels. At higher electric fields, transport in disordered materials like doped MOSs can no longer be described by an Ohmic law, but its current versus voltage characteristics (I–V) assumes a parabolic shape that can be described by the space-charge-limited current (SCLC) model (6)

$$I = A\,\mu_{eff}\,\varepsilon\frac{V^2}{L^3} \quad (6)$$

where A is a geometry factor, μ_{eff} is the effective mobility of charges, ε is the permittivity of the material, V is the potential applied over the sample thickness L. Such model was originally developed to describe charge transport in insulating materials[67] but its validity has also been demonstrated for compound materials like amorphous InGaZnO (a-IGZO),[68] rutile titanium oxide,[69] and hybrid organic–inorganic perovskites.[70] These models will find suitable application as explained at the end of Section 2.2.

2.2. Advanced Structural and Functional Characterization of Doped MOSs

The knowledge of the doping-induced properties of MOSs allows designing devices that exploit the major advantages of the materials involved to maximize their performance. In this section, we focus on the advanced characterization available worldwide for responding to the modern technological demands. We group the most important ones into five categories (the 5W chart, see **Figure 5**), each one addressing a specific task:

1) the determination of the chemical nature and the of the actual oxidation state of the dopant once incorporated into the matrix (WHO);
2) the determination of the quantity of dopants within the matrix (WHAT);
3) unveiling the actual arrangement (either interstitial or substitutional) of the doping element/ion into the host matrix, i.e., its chemical environment and coordination geometry/number (WHERE);
4) the understanding of the interaction between the host matrix and the dopants in terms of charge carrier dynamics (WHEN);
5) the effect of incorporation of the guest species on the functional properties of the host compound, i.e., mostly electrical, magnetic, and optical ones (WHY);

All five points are relevant in structure–properties relationships determination, therefore an effective approach to a thorough characterization of the dopant/matrix system is pivotal to improve, in an iterative loop, the synthesis routes to prepare better performing doped MOSs. In this framework, all these tasks might be profitably addressed by using different characterization methods, delivering complementary and mutually integrating information related to composition (intended as chemical state, chemical environment, and atomic percentage of the dopant), microstructure and morphology. The presented scheme therefore outlines the interplay among the different analytical tools along with the main delivered pieces of information, that we discuss deeper in the following lines.

WHO & WHAT: the chemical nature and the oxidation state of the dopant is the first fundamental evidence to obtain. As previously discussed, unlike group IV or group III–V semiconductors, the doping content in MOS is often exceeding a few percentage points with respect to metal content. This is intrinsically relaxing the requirements for the synthetic control of dopants concentration and the need of ultrafine characterization techniques. On the other hand, high heteroatoms contents

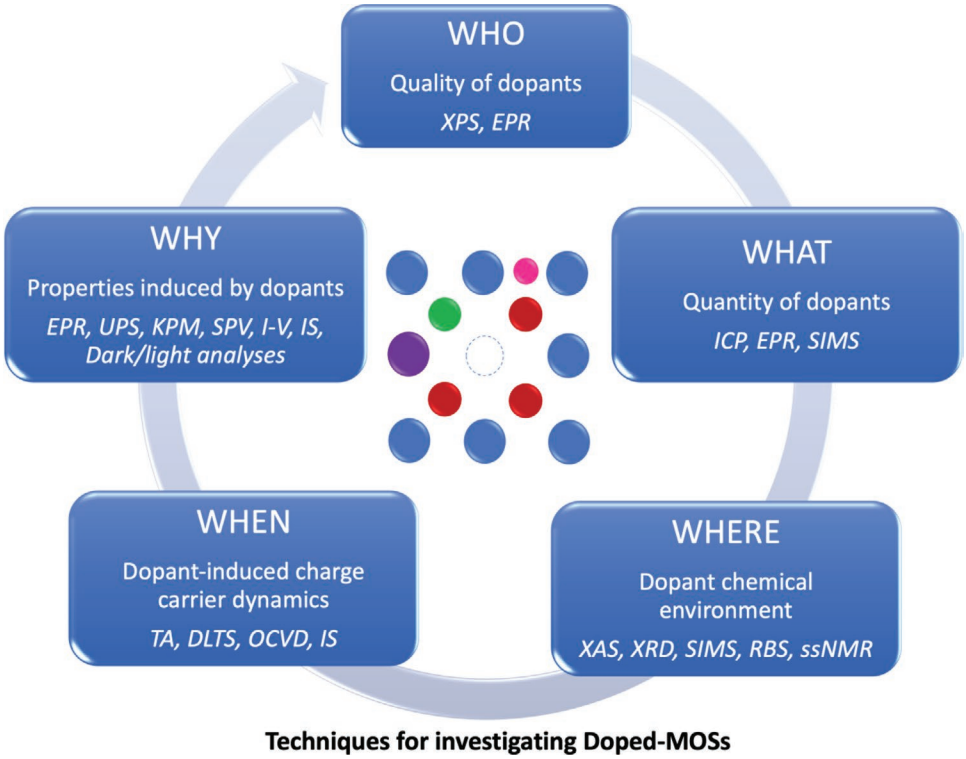

Figure 5. The 5W chart of the doped MOSs investigation techniques discussed in this section. Acronyms are clarified in the text.

may result in unpredictable modification of the material's physical and chemical structure, thus an accurate determination of the dopant chemical state (nature of the element, oxidation state, chemical environment) and atomic percentages of the different elements within doped-oxide are essential to obtain reproducible results in terms of functional performance. Such information can be obtained by an X-ray based method, i.e., X-ray photoelectron spectroscopy (XPS),[71] a well-established, versatile and surface sensitive spectroscopic technique for the study of surfaces (i.e., the first 2–10 nm) of powders and thin films. Being a well-established analytical technique, a lot of literature is available regarding doped MOSs. However, for the purposes of this perspective, we want to emphasize the use of XPS for estimating, for example, the stoichiometry of doped films (like in the case of Al:ZnO[72] and Cs:TiO_2[73]), or even to perform depth profiling analysis (**Figure 6**a).[74] Inductively coupled plasma (ICP) is considered the benchmark tool for the determination of traces amount of guest species inside the host lattices up to the ppb level: in our recent paper, for instance, we correlated the nominal doping concentration of V cations inside MoO_3 and CO_3O_4 host species.[75] There are many other analytical methods providing quantitative/semiquantitative information on the concentration of guest species such as EPR,[76] UV–vis (through the determination of the transparency),[77] XPS[78] and so on.

WHERE: particular attention must be given to the study of the chemical environment of the dopants, since it is the mutual interdependency between host and guest material that positively or negatively affects the final performance of the device. Whether a dopant is embedded either as interstitial or as substitutional ion in the host matrix can be unraveled through highly locally-specific methods, providing insight into the atomic length scale, either directly (through determination of coordination environment, i.e., type and number of neighboring ions, and length distances) or indirectly, through EPR. As far as the former methods are concerned, the most powerful one is surely X-ray absorption spectroscopy (XAS),[79,80] based on X-ray/matter interaction, delivering local order information starting from the analysis of the complete XAS spectrum, which can be divided into two portions: the near-edge part (usually within 30–40 eV from the edge), called X-ray absorption near-edge structure (XANES), whereas the extended oscillatory spectrum is named extended X-ray absorption fine structure (EXAFS). When an X-ray beam passes through a material, the intensity of the outgoing beam I is modulated by the absorption characteristic of the material itself (related to the absorption coefficient μ), following the Lambert–Beer's law. This oscillatory modulation of the X-ray absorption coefficient near and above an X-ray absorption edge provides information on the chemical, and electronic features of the absorbing element. The accurate analysis of XAS data provides indeed relevant information, such as coordination numbers and geometry of absorbing atoms, as well as bond distances between these and their neighbors. The use of XAS to track the typology of ion/element insertion within the host matrix has been broadly used to unveil whether a doping ion arranges itself by replacing a host matrix atom in the lattice (substitutional) or occupies a void within the lattice (interstitial): substitutional and interstitial iron was found in Fe-doped NiO through EXAFS,[81] whereas XAS was used to track oxygen vacancies in TaO_x[82] or the structural transformation from CoO to Co_3O_4 (Figure 6b).[83] Furthermore, in the work of Niedermeier et al.[84] dealing with magnesium

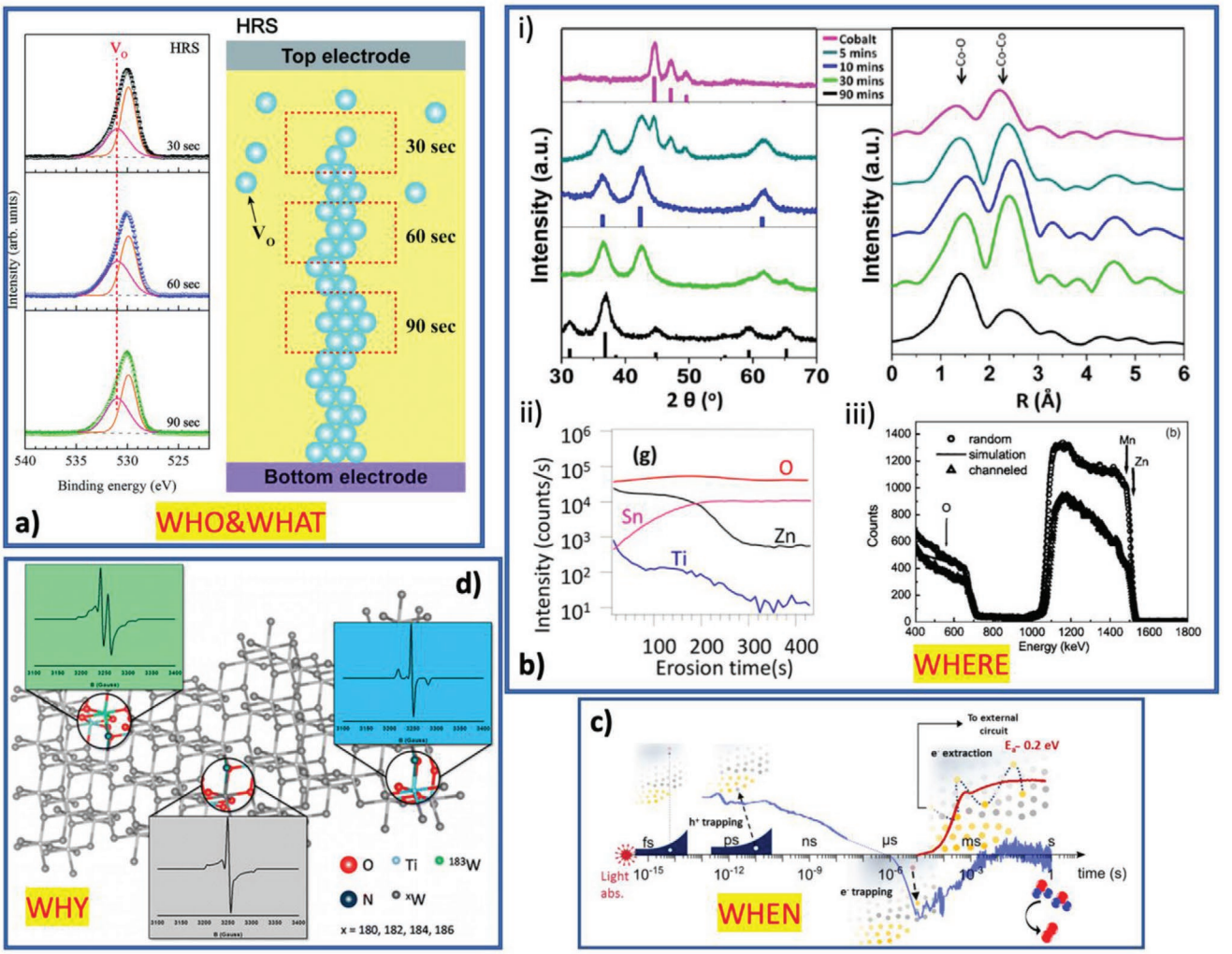

Figure 6. a) WHO&WHAT panel: by XPS depth profiling, a gradient in the oxygen vacancy concentration is found. Adapted with permission.[74] Copyright 2019, Royal Society of Chemistry. b) WHERE panel: i) XRD (on the left) and the Fourier Transform of EXAFS data EXAFS (on the right) analyses allow to follow the structural conversion from CoO to Co_3O_4. Adapted with permission.[83] Copyright 2013, American Chemical Society. ii) Host metal species tracked by SIMS. Adapted with permission.[99] Copyright 2019, American Chemical Society. iii) Mn-doped ZnO compound investigated by RBS. Reproduced with permission.[100] Copyright 2005, American Institute of Physics. c) WHEN panel: TA technique allows to study the charge carrier trapping and electron transport in metal oxides. Reproduced with permission.[114] Copyright 2019, American Chemical Society. d) WHY panel: EPR helps to estimate the photoactivity performance of doped metal oxides. Reproduced with permission.[152] Copyright 2013, American Chemical Society.

oxide nanoparticles with added mixtures of iron or cobalt ions, XAS was used to evaluate the coordination and symmetry around the transition-metal ions and to determine their actual oxidation state as a function of the synthesis conditions, as well as to point out a significant segregation of Fe ions into low-coordinated sites. In a further recent work,[85] the aliovalent substitution mechanism and crystal structure of Eu^{3+}:$CaMoO_4$ and Eu^{3+},Na^{+}:$CaMoO_4$ phosphors was addressed using complementary techniques like Raman spectroscopy and XAS. The authors evidenced, by exploiting the local atomic sensitivity of XAS, that the substitution mechanism in the two systems was different. [86]

The insertion of doping elements/ions might in some cases determine also detectable distortions/rearrangement in the host matrix lattice, which can be evidenced by tracking lattice parameters changes. X-ray diffraction (XRD) provides a convenient and practical means for the identification of crystalline compounds. In addition, XRD, typically supported by Rietveld refinement,[87,88] can indeed provide also relevant information concerning the occupancy of dopant atoms, the crystalline structure of the host lattice as well as lattice deformation upon doping.[89,90] In a recent study,[91] the Rietveld refinement of the X-ray diffraction pattern allowed to unveil the modifications of wurtzite ZnO structure upon doping with Ce, Fe, Co ions. In a further example,[92] dealing with Mg/Mo co-doped thermochromic vanadium dioxide nanorods, an increase in the intensity of the Bragg peaks of Mg-doped VO_2 was observed with increasing dopant concentration, which was ascribed by the authors to an increasing in the VO_2 crystallinity by increasing the dopant level. In a further contribution,[93] XRD analysis of $V_{1-x}W_xO_2$ films evidenced how the reflections were shifted to smaller angles, indicating a small enlargement of the crystal

planes distances as predictable for $V_{1-x}W_xO_2$ films because W has a larger atomic radius in comparison with V. An even higher resolution can be achieved by employing synchrotron light-assisted XRD. Whenever the investigation of doped MOS thin films is required, a valuable tool is grazing incidence XRD (GIXRD)[94] where, thanks to grazing configuration, the small intensity derived from limited sampling is maximized and the structural parameters of surfaces and interfaces can be determined through the comparison between the experimental and calculated structure factors.

Whenever doping in thin films has to be investigated, and in particular dopants in-depth distribution, two complementary methods come in play, i.e., secondary ion mass spectrometry (SIMS)[95] and Rutherford back-scattering spectrometry (RBS),[96] both delivering information on in-depth distribution of targeted species. In a SIMS analysis, the surface of the sample is bombarded by a focalized beam of primary ions accelerated with at an energy ranging between 0.5 and 20 keV. As a consequence of the energy transferred by primary ions, atoms are removed from the surface and a fraction of the ejected atoms is ionised thus producing a secondary flux, of both positive and negative ions, having a mass/charge ratio and an isotopic pattern which are characteristic of the chemical nature of the element. In addition to surface analysis, this technique may also be used to establish concentration profiles as a function of depth. Through ion milling, successive atomic layers are removed, and surface compositional analysis are performed during this progressive erosion. The analysis of these ions leads to identification of the surface ion fragments, thus enabling to monitor in-depth distribution of dopants and impurities and additionally to investigate surface phenomena, such as absorption, corrosion, and diffusion and has shown its potentiality to identify chemical species. High sensitivity, isotopic discrimination, atomic, molecular and cluster ion detection have highlighted the role of SIMS in the analysis of major and minor components on the surface or in the bulk of materials and evaluating their distribution in the inner layers. In particular, SIMS has been widely applied to follow the in-depth profile of the distribution of different species within a thin film or coating, also of doped MOSs.[97] Whenever the profile of the host metal species and the one of the dopants have a similar behavior, a homogeneous distribution of the latter in the former can be inferred, as outlined in several examples reported in the literature (Figure 6b).[98,99]

A similar information, i.e., the in-depth distribution of doping ions into a metal MOS thin film can be retrieved by RBS depth profiling. RBS is a nuclear-based method used for the surface films. A metal target is bombarded with ions at an energy in the MeV range (typically 0.5–4 MeV), and the energy of the backscattered projectiles is recorded with an energy sensitive detector. Being the backscattering cross section for each element a known quantity, the method enables a quantitative compositional depth profile without the need for reference samples. The method is moderately nondestructive, has a good depth resolution of the order of several nm, and a very good sensitivity for heavy and efficiently backscattered elements of the order of parts-per-million (ppm). For example, the structural disorder of a Mn-doped ZnO lattice was studied through RBS in which the amount of substitutional Mn centers was characterized (Figure 6b),[100] or the accurate stoichiometry upon silver doping in a CuO thin film[101] could be determined by RBS.

Elements distribution at the nanoscale can also be thoroughly monitored by electron microscopy. Structural information is provided by high resolution transmission electron microscopy (HR-TEM), allowing for the determination of doping-induced lattice distortion and heterostructures. Atomic-resolution elemental mapping can also be achieved by exploiting TEM-related spectroscopy techniques.[102] Energy dispersive X-ray spectroscopy[103] (EDS) and electron energy loss spectroscopy[104] (EELS) are among the most employed techniques to retrieve direct information on the localization of doping atoms in metal oxides.

We have discussed in Section 2.1, how the presence and distribution of oxygen is extremely relevant in affecting the surrounding metal environment. For this reason, the tracking of isotopes would represent a valuable alternative for a detailed characterization of doped MOSs. Solid state nuclear magnetic resonance (ssNMR) is the suitable method for achieving this goal.[105–107] In a recent work,[108] ^{17}O-ssNMR was applied to unveil the different behavior of oxygen ions at the surface of CeO_2 nanoparticles with respect to the bulk; in another work,^{27}Al-ssNMR was applied for clarifying the site and the chemical environment in Al-doped ZnO.[109] Furthermore, ^{119}Sn-ssNMR was used for the characterization of fluorine-doped tin oxide (FTO) nanoparticles in combination with Mössbauer spectroscopy,[110] a powerful technique that allows to obtain highly resolved information on the chemical composition of nearest neighbors in a lattice.

Concerning the dynamics, time-scale is important when discussing electrical/optical traps in semiconductors. Therefore, the role of vacancies in MOSs is particularly interesting when considering photoactive media, like in wurtzite (ZnO),[111] hematite (Fe_2O_3),[112] TiO_2,[113] or $BiVO_4$ (Figure 6c)[114] which act as photoanodes for water splitting. In this case, the concentration of oxygen vacancies affects the photocatalytic behavior of the entire device by improving the overall power conversion efficiency, PCE, (boosting the n-type conductivity), but also limiting it by increasing the charge recombination centers (i.e., electrical/optical traps).[115] Generally in such devices, the conductivity is limited, mainly due to polarons, i.e., self-trapped charge carriers.[116] Transient absorption (TA) spectroscopy coupled to theoretical calculations provides information on the energetics of charge traps within the bandgap of the absorber material in contact with ancillary layers or electrolytes, like the tracking of the carrier loss pathway for nanocrystalline hematite for instance.[117] If such techniques are applied to thin films of MOSs, it is possible to directly probe the materials in an opto-electronic device architecture. However, basic research is also performed on MOSs colloidal suspensions in order to acquire fundamental knowledge on electron–holes kinetics at the nanoscale.[118]

Combining optical and electrical characterizations is a good strategy for gaining deeper information on defects dynamics.[119] In this context, one the most powerful characterization technique is the deep-level transient spectroscopy (DLTS) that, performed at various temperatures, can be used to gain information about the energy levels in the bandgap of a semiconductor. The basic principle of the DLTS technique consists of

measuring the time-dependent variation of the sample capacitance (C-DLTS) or current (I-DLTS) due to a stepped change in the voltage bias that brings the devices under analysis from a "trapped state" (where all the trap states are occupied) to a "detrapped state" (where all the trap states are empty). When the device changes its status from the trapped state to the detrapped state, the thermally activated trap states progressively get empty, leading to a transient response whose time constant τ decreases by increasing the temperature. Since the transient time constant depends on the position of the trap state in the semiconductor bandgap, following the Shockley-Read-Hall generation and recombination theory,[120] the Arrhenius plot of $\ln(\tau)$ versus T^{-1} allows determining the energy level of the specific trap states. That is the case, for instance, of classic GaN and AlGaN semiconductors in which the extensive use of DLTS led to the realization of a big database that allowed to correlate the trap states at a given energy level with the presence of defects, impurities and dopants within the semiconductors.[121] The DLTS technique is currently intensively implemented to investigate defects in crystalline semiconductors, but its efficacy has been also investigated in organic semiconductors[122,123] and a-IGZO[124] paving the way to the use in doped MOSs for the creation of specific databases of subgap states (both density of states and traps) that will help in the development of this new class of materials.

Transient measurements can also be applied for the investigation of recombination processes within the semiconductor and at its interfaces. That is the case of open-circuit voltage decay (OCVD) in which an excess of charges is injected either by illumination (e.g., in the case of a solar cell) or by the application of a forward bias (both in solar cells and raw materials).[125] To distinguish between the two kinds of voltage decays, they are usually referred as OCVD and ABVD (after-bias voltage decay). Here we will not make such distinction and we will refer to these techniques simply as OCVD.

Before the recording of OCVD transients, excess carriers are injected (either optically or electrically) until the sample reaches its steady states. Then, the excess carrier source is switched off and, while the sample is kept in open circuit, the OCVD transient is recorded during time. OCVD transients feature exponential decays $\approx\exp(-t/\tau_b)$ that is associated with the recombination rate of the excess carriers, with τ_b being the carrier lifetime. However, experimental voltage decays of PSCs with a metal-oxide transport layer can show up to three exponential contributions (7)[126]

$$\Delta V_{OC}(t) = A_1 \exp\left(-\frac{t}{\tau_{b_1}}\right) + A_2 \exp\left(-\frac{t}{\tau_{b_2}}\right) + A_3 \exp\left(-\frac{t}{\tau_{b_3}}\right) \quad (7)$$

Where τ_{b_1} = 10–100 µs and τ_{b_2} = 1–100 ms were associated with charge discharge and recombination, respectively, whereas a slow component τ_{b_3} up to 100 s was associated to the ionic polarization/depolarization kinetics. It is furthermore worth noting that other works reported a two-exponentials decay with lifetimes in the order of few µs,[127] highlighting the range of variability in this class of devices. This phenomenon was also highlighted by Ravishankar et al.,[128] who fabricated PSCs using three different metal oxide transport layers (namely FTO, compact-TiO_2, and mesoporous TiO_2) thus demonstrating how the transport layer plays a crucial role in determining the devices performance, investigating charge accumulation, and recombination at the interfaces.

Under the perspective of investigating how MOSs impact on the overall performance of PV and energy storage devices, impedance spectroscopy (IS) becomes a powerful tool to reveal the interaction between several layers in a device. IS consists of measuring a device complex impedance at a wide range of frequencies, and the results are usually reported in a Nyquist plot that shows the imaginary part versus the real part of the measured impedance. Data are then fitted by an equivalent circuit model that is usually composed by passive elements such as resistances and capacitances whose values can then be related to physical parameters of the material in the device (e.g., thickness, dielectric constant, conductivity).[129] The same impedance measurement can be performed at different applied biases to give an overview of the device at all its operating conditions.

WHY: the knowledge of the energetics of doped MOSs is essential for a proper design of optoelectronic devices. While an ab initio prediction of the band structure may provide a valuable tool for the choice of a MOS for a specific application,[37] the use of such prediction tools for understanding the role of doping elements on MOSs energetics is more challenging[130] due to the need of a full understanding of dopant nature, concentration, and distribution, as previously discussed. For example, whether or not dopants are incorporated into the material rather than being adsorbed on the surface, directly affects their optical spectra and indicate a strong impact on their electronic structure in general.[131] This is particularly important on the nanoscale, where the samples provide a large surface-to-volume ratio. Strategies for dopant incorporation rather than dopant segregation will directly improve their optical and electronic properties.[132] Additionally, the presence of oxygen vacancies in metal oxides will ultimately enhance carrier scattering at the doubly charged vacancy sites.[133] Also Fermi level, work function and ionization potentials, which are closely linked, are strongly affected by the level and type of doping and will ultimately modify band gaps and energy band alignments.[134] As a consequence, a thorough characterization of the materials underlying optical and electronic features upon doping is needed to provide a causal relation between doping and functional properties, eventually resulting in the optimization of the device performance.

A combination of techniques must be considered that first study the position of the bands and, second, investigates the kinetics of charge carriers. Ultraviolet photoelectron spectroscopy (UPS) combined with Kelvin Probe (KP) microscopy allows getting information on the position of the valence band (VB) and the Fermi level in a semiconductor. Usually applied to molecules, the techniques are nowadays largely applied also to *pn* junctions in order to determine band bending phenomena occurring at the interfaces. Briefly, if a dopant (a neutral atom, an ion, or a compound) is added in the host material, a change in the relative position of the orbitals constituting the VB may occur. Exploiting the Einstein's photoelectric effect, in principle one can probe the Fermi level shift upon doping of a material,[135] and combining this information with the work function/charge carrier concentration obtained by KP[136] and/or the optical band gap determined by UV–vis spectroscopy (see later

in the text), is easy to build an energy diagram. A recent work of some us describes the fine tuning of the work function (WF) of vanadium-doped Co_3O_4 and MoO_3 mesostructures at different concentrations of the guest species.[75] Kumar et al., using an external bias, tuned the WF of Al-doped ZnO[137] following the process through KP microscopy. Generally, when designing optoelectronic devices, UPS and KP analyses are fundamental both for making predictions on the overall performances and for proper designing the MOS doping strategy, in combination with calculation, as it was the case for the estimation of self-doping of the TiO_2 (110) surface.[138] Moreover, intensity-modulated surface photovoltage (SPV) measurements allows to determine the SPV in thin films, a parameter that is strongly affected by the presence of defects and requires higher sensitivity than the usual steady-state KP measurements.[139]

In order to assess PV performance, current–voltage (*I–V*) characterizations can be successfully implemented for the extrapolation of the effective carrier mobility in the semiconducting materials. Moreover, *I–V* characteristics are a powerful tool to investigate nonidealities, such as hysteresis that may alter the transport properties of the material and, in turn, affect PV devices efficiency and stabilities,[140] a huge problem that researchers are encountering, for example, when dealing with PSCs [141,142] where *I–V* measurements performed at different scan rates can elucidate the SCLC transport mechanism assessing the role of mobile ions in the device conductivity. Current versus voltage characteristics can also be combined with optical analysis to gain further information on the MOSs properties. These analyses are of fundamental importance while developing materials for the next generation photovoltaic applications. In general, two kind of optical analysis can be performed: a) light emission imaging; b) light adsorption measurements. Performing light emission imaging onto a MOSs film allows to i) draw a map of radiative recombination sites (visible spectra imaging) that can negatively contribute to the efficiency of the final PV cell; ii) identify the presence of defective hot spots (infrared imaging) that are the major and most severe cause of failure in state-of-the-art solar panel.[143] On the other hand, light adsorption measurements are performed by illuminating the sample under analysis while recording *I–V* characteristics. When using the nominal solar spectrum, these measurements give the actual efficiency of the PV system, however monochromatic illuminations can be used to characterize the single MO. Furthermore, they can provide the material external quantum efficiency (EQE) that can then be combined with its adsorption spectrum to optimize the overall efficiency of the final PV system. An example can be found in the emerging perovskite/Si tandem solar cells that, combining the adsorption spectra of the two PV materials, reached the outstanding efficiency of 29.5%.[55] On the other hand, the spectral adsorption analysis can be concentrated in a very small light spot that, similarly to the light emission imaging, can be used to check the quality of the MOS film detecting the presence of defects and impurities by drawing an EQE map.

Thanks to its large versatility, impedance spectroscopy (IS) is implemented in a variety of different applications[129] that range from modeling of PV devices and understanding charge transport at the interfaces with different materials (e.g., between photoactive layer and transport layers),[128,144] to the study of the sensing mechanism of gas sensing devices by investigating how the impedance parameters change during the devices operation.[145,146] Another important use of IS can be found in the investigation of degrading phenomena in material and devices. For instance, by measuring the evolution in time of the impedance equivalent circuit parameters, IS has been successfully implemented to investigate the degradation of CuO in ion batteries[147] as well in the degradation of $TiO_2/MAPbI_3$ interface in solar cells.[148]

Finally, EPR spectroscopy is often used for characterizing the structure and the electron spin density distribution of given paramagnetic centers, even at low concentration.[149] Briefly, the technique consists of probing the interaction between the quantized electron magnetic moment of a paramagnetic species and an external applied magnetic field. In MOSs, this property is particular interesting when considering point defects in wide band gap materials like TiO_2, ZnO, or ZrO_2: as typical case-study, different authors examined the interstitial nitrogen center in titania, unraveling its tridimensional configuration,[150] its photosensitivity character,[151] and the correlation with other dopants like, for example, W (Figure 6d)[152] and B.[153] There is a huge variety of EPR studies focusing on the functional role of the dopant in MOSs, like Cu/Ni inclusions in ZnO,[154] the effect of gamma rays irradiation on CeO_2 glasses upon lithium cations doping[155] or the boosted conductivity in Ga-doped ZnO powders.[156]

3. Use of Doped MOSs in Light-Harvesting Technologies

The use of doped MOSs for light conversion applications, with particular focus on the case of earth abundant species, is critically discussed in this paragraph. The section is further divided into two subsections in order to distinguish between cases in which doped MOSs act as the main active materials in the light conversion process (photoelectrochemical production of solar fuels, all oxide solar cells, multicharge accumulation in MOS nanocrystals) from those in which they act as ancillary items to other species carrying out the actual light harvesting (dye-sensitized and perovskite solar cells, photon up/down-conversion). **Table 2** summarizes all the MOS host lattices, with the relative dopants and pursued functional property changes, discussed in this whole chapter.

3.1. Doped MOSs as Active Materials in Light Harvesting Technologies

3.1.1. Doped MOSs as Photoelectrocatalysts

One of the most prominent applications for MOSs in light-conversion consists in the photocatalytic conversion of low-value-chemicals into those of higher value, such as solar fuels or industrially relevant compounds. Among the plethora of possible chemical reactions, water splitting is prominent due to its apparent simplicity and the tremendous impact on the energy market.[196] The practical implementation of solar to hydrogen devices is challenged by a number of strict requirements for

Table 2. Summary of MOS host lattices and relative dopants discussed for specific functionalities enhancement across this chapter.

MOS Host lattice	Dopant	Functionality/application	Ref.
$BiVO_4$	Oxygen vacancies	Photoelectrochemistry	[114]
$CaMoO_4$	Eu	Phosphors for lighting and light-conversion	[85]
CeO_2	Li	Gamma rays	[155]
Co_3O_4	V	Work Function engineering	[75]
	Oxygen vacancies	Understanding of charge diffusion mechanism	[83]
Cu_2O	Bi Zn Ni Cl	Charge carrier increase	[157–160]
CuO	Ag	Photocatalysis on flexible substrates	[101]
Fe_2O_3	Oxygen vacancies	Photoanode engineering for photoelectrochemistry	[112,117]
	Ti Pt Si Sn Mg	Photosensitivity	[161–167]
HfO_2	Yb + Tb	Spectral conversion	[168,169]
MoO_3	V	Work function engineering	[75]
NiO	Fe	Structure modification	[81]
SiO_2	Ag + Yb	Broadband sensitization	[170]
SnO_2	La	Spectral conversion	[171]
Ta_2O_5	Al	Photosensitivity	[172]
	Oxygen vacancies	Memristor technology	[82]
TiO_2	Cs	Work function engineering	[73]
	Oxygen vacancies	Interface engineering	[113]
	N	Photosensitivity	[151,173]
	W	Photosensitivity	[152,174]
	B	Photosensitivity	[153,173]
	P	Photosensitivity	[173]
	Zr Nb F Y	Photosensitivity	[175–178]
	Er, Yb, Eu	Spectral conversion	[179]
VO_2	Mg, Mo	Thermochromic properties	[92]
WO_3	Fe	Photosensitivity	[180]
	Oxygen vacancies	Photoelectrochemistry	[111]
ZnO	Al	Thermoelectrics Work function engineering Protective layer	[72,109,137,181]
	Ce, Fe, Co	Ferromagnetism	[91]
	Mn	Ferromagnetism	[100]
	Ga	Electrical conductivity improvement	[156]
	Co	Photosensitivity	[182]
	Al Fe	Electron blocking properties Light-driven supercapacitor	[183–185]
	Mn	Photocatalysis	[186]
	B Co Ga Sn Ti Cu	Decreased charge recombination	[187–191]
	Al	FTO replacement	[192,193]
	La	Downshifting and scattering in PSCs	[194]
ZrO_2	Ag + Yb Ag + Tb + Yb	Broadband spectral conversion	[170,195]

the materials acting as the "core" of the artificial photosynthesis process. In this regard, MOSs have been widely considered as the archetype class of materials due to attractive combinations of suitable optical gaps and large resistance to corrosion.

Without having the presumption of addressing this extremely wide field, which was already thoroughly reviewed,[197–202] we choose to focus on the importance of the choice of the main photocatalytic element. Indeed, within this specific application field, the use of cheap and widely available elements represents the only feasible economical perspective due to the large amount of catalyst needed, especially if compared to the closest relative, i.e., water electrolysis. It has been previously estimated that a solar to hydrogen devices requires 50–200 times the amount of active material needed for a conventional electrolyser.[199] As a consequence, the use of precious or heavy, toxic metals is both economically and environmentally unviable and earth-abundant MOSs are ideal candidates to fulfill such requirements.

Among the commonly employed photocatalytic approaches,[203] i.e., the colloidal-phase photocatalytic (PC) approach and the photoelectrochemical (PEC) approach, the latter allows for a modular development of materials specifically suitable for photocathodes or photoanodes in separate environments, before combining them into a single water splitting device. This is particularly important for MOSs,[204] since their valence band position is often driven by highly positive O 2p orbital (+3.0 V vs normal hydrogen electrode, NHE), thus limiting the maximum reduction potential obtained with a photoexcited narrow bandgap oxide. As a consequence, overall water splitting is rarely achieved with a single MOS, but rather by fashioning complex Z-scheme photocatalytic heterostructures or bias-free tandem photoelectrochemical systems (**Figure 7**a).

Wide bandgap MOSs, such as TiO_2, ZnO, and Ta_2O_5 exhibit intrinsic n-type doping and a large charges diffusion length, highly desirable properties for a photoanode material. However, the lack of visible light absorption limits their application in specific applications such as water purification employing

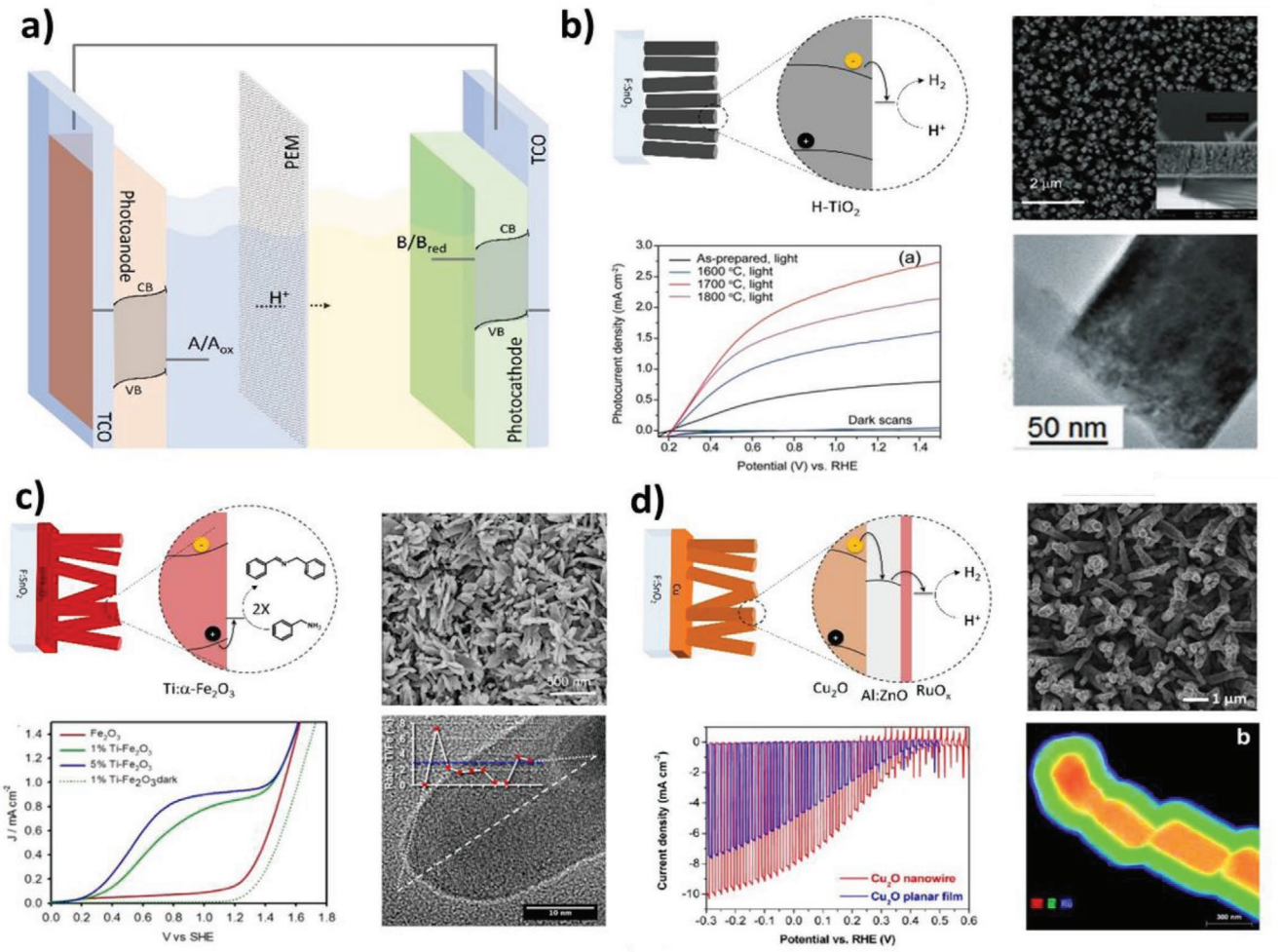

Figure 7. Schematic drawing of a Tandem PEC cell a) and most representative examples of earth abundant doped photocatalysts taking advantage of doping-related PEC enhancement. b) Hydrogenated black TiO_2 exploiting the defect-induced bandgap narrowing to increase the visible-light activity as photoanode for OER. Adapted with permission.[207] Copyright 2019, Wiley. c) Improved charges diffusion length in Ti-doped a-Fe_2O_3 nanowires employed as photoanode for the oxidation of an organic molecule (benzylamine) into an industrially relevant compound (*N*-benzylidenebenzylamine). Adapted with permission.[163] Copyright 2019, Elsevier. d) Enhanced stability of a nanostructured Cu_2O photocathode for HER resulting from a thin conformal coating with Al-doped ZnO. Adapted with permission.[213] Copyright 2016, American Chemical Society.

artificial UV light source. The most employed approach to overcome this issue relies on the sensitization with an organic dye[205] or a second semiconductor. In addition, intrabandgap states can be produced through extrinsic metal[206] and non-metal doping,[173] as observed by introducing B, N, or P into TiO_2 anatase phase, or by introducing hydrogenation-induced oxygen vacancies,[174] obtaining the so-called "black titania," named after the broad visible absorption spectrum resulting from the reduced band gap (Figure 7b). Similarly, visible-light absorption is promoted in "gray Ta_2O_5" by Al-doping,[172] as well as in Fe-doped WO_3[180] and the more fancy "green ZnO," resulting from Codoping.[182] Despite the promising premises of this approach and some interesting application examples,[207] their practical employment as photoanodes is hindered by the localized nature of the intrabandgap states and the introduction of lattice distortion-dependent recombination centers, reducing the diffusion length of the photoinduced holes.

Intrinsic visible light absorption is natively encountered in several transition metal oxides such as α-Fe_2O_3 (bandgap ≈2.2 eV), more common as hematite, whose striking abundance and stability have attracted large attention since the beginning of the field. However, pure hematite photoanodes achieve average solar water oxidation photocurrents much lower than the theoretical maximum for the corresponding bandgap, i.e., ≈12 mA cm^{-2}. The poor polaron conductivity limits the photoinduced charge separation in pure hematite to few nm, increasing the charge recombination probability and reducing the photocurrent. Among the possible semiconductor engineering approaches, doping with transition metals such as Ti,[161] Pt,[164] as well as other elements like Si,[165] Sn,[166] and Mg has been observed to largely improve hematite performance as photoanode, even if the photocurrent improvement mechanism is still under debate.[167] Ti-doped α-Fe_2O_3 photoanodes, above all, not only achieved an impressive 2.5 mA cm^{-2} maximum photocurrent at 1.23 V versus

RHE without the addition of co-catalyst or surface treatment,[162] but they have also been employed for alternative oxidation reactions. For instance, in a recent study published by some of us,[163] nanostructured Ti-doped hematite photoanodes were demonstrated to convert benzylamine to *N*-benzylidene benzylamine with almost unitary Faradaic efficiency and photocurrent up to 1.2 mA cm^{-2} (Figure 7c). In the same work, hydrogen was produced at the counter-electrode with the addition of an external bias as low as 0.6 V.

Interestingly, the second most employed and currently most popular photoanode material for PEC cells is $BiVO_4$, a ternary semiconductor displaying visible-range absorption and relatively large charges diffusion length. $BiVO_4$ provides interesting activity as photoanode for the oxygen evolution reaction (OER)[208] and organic oxidation reactions,[209,210] often surpassing the one displayed by hematite counterparts, but its main limitation lies within its composition. Despite being often considered as an earth-abundant element, Bi is a relatively scarce element and included among CRMs,[5] being only the 71th element for availability on earth crust and displaying one of the highest supply risk indicator.[211] Its practical employment in PEC and photocatalytic devices is therefore conflicting with the geopolitical and environmental aforementioned issues.

There is a general lack of p-type visible-light absorbing MOSs, but their development is highly desired due to the need for efficient photocathodes for PEC water reduction, to be employed in tandem two-electrodes devices together with the aforementioned photoanodes. Cu-based binary and ternary oxides are currently the most earth-abundant promising solution,[212] with Cu_2O leading the way, but they usually suffer from low photovoltage and rapid photocorrosion. In a seminal work,[181] the use of protective layers like aluminum-doped ZnO and TiO_2 allowed a tremendous enhancement of Cu_2O stability, but limited performance (Figure 7d). This result, already improved by nanostructuring the Cu_2O layer,[213] was then outperformed by introducing a band-aligned buried p–n junction with Ga_2O_3, allowing for >100 h stability and about 1 V photovoltage.[214] In addition, these results were further enhanced by introducing a Cu-based hole transport layer.[215] Unlike previous examples, Cu_2O doping has been rarely employed as a strategy to improve the PEC performance due to the limited enhancement observed in the few attempts reported. Indeed, the carrier concentration improvement observed by doping with transition metals such as Bi,[157] Zn,[158] and Ni[159] did not result in a significant improvement of Cu_2O photocathodes. On the other hand, doping with halogens like Cl,[160] often unintentionally introduced in Cu_2O lattice,[216] might result in undesired n-type characteristics. Despite that, the recent interest revival on Cu_2O and associated ternary oxides[217] proves the need of active research in the field and suggests further development on doped Cu_2O structures for PEC implementation.

3.1.2. Doped MOSs in All-Oxide Solar Cells

The idea to produce an operating all-oxide solar cell dates back almost 40 years, based on the concept to apply cheap, earth-abundant and environmentally friendly materials. Pioneering studies developed solar cells by thermal oxidation of copper bulk sheets, in which transparent conducting layers were subsequently deposited to obtain a p–n junction.[218] Such technology is however unsuitable for scale-up purposes, due to a series of shortfalls: the high temperature required to produce high-quality oxide surface layer (T > 1000 °C) and the need to use high-purity and expensive Cu foils.[219] In addition, the overall efficiency is rather limited (on average around 2%), even if interesting results were achieved for top efficiency cells (PCE≈8.1%).[220] For this reason, despite the fact that appreciable results were obtained in terms of PCE, with max PCE around 6–8%,[221] the research moved toward the development of thin-film-based homo- and heterojunctions, produced through a series of different techniques, including electrodeposition,[222,223] physical vapor deposition,[224,225] atmospheric atomic layer deposition,[226] spray pyrolysis,[227] and wet chemistry[228] through chemical coprecipitation or sol–gel.[229]

One of the main challenges in all-oxide PV is the very low mobility of holes in most of the p-type light absorbers,[230] which leads to high charge recombination, impairing the charge collection and the overall PCE. One effective strategy to modulate the optoelectronic properties of thin films is doping.[229]

Up to now, copper oxides (relatively uncritical MOSs) dominated the research on oxide solar cells, mainly due to the favorable energy gap of Cu_2O (E_g≈2.1 eV)[231] and CuO (E_g≈1.4 eV),[232] close to the ideal gap maximizing the reachable PCE, according to the Shockley–Queisser limit.[233] Mimicking Si solar cells, the possibility to obtain a copper oxide homojunction was explored.[234] p- and n-type doping were induced in Cu_2O thin films produced by electrochemical bath deposition in a three-electrode electrochemical cell, by using an aqueous solution containing 0.1 M sodium acetate and 0.01 M cupric acetate for the n-type layer, and through a sulfidation process, by exposing the copper sulfides layer to ammonium sulfide gas to induce a p-type doping. However, while a reasonably high short circuit photocurrent density (J_{sc}) was achieved (12.4 mA cm^{-2}, among the highest for all-oxide solar cells), an overall efficiency below 1% was obtained, mainly limited by the low open circuit photovoltage (V_{oc}, about 287 mV), and fill factor (FF, about 25%).

An alternative to homojunction device is the heterojunction thin film configuration, in which either TiO_2 or ZnO (both with E_g≈3.2 eV) are mainly applied as n-type wide bandgap semiconductors, in combination with copper oxide and other optically active layers. In such configuration, rather than doping, the key point is to create a suitable electronic band structure, able to induce exciton separation at the depletion region of the p–n junction, driving holes and electrons in the right direction, simultaneously inhibiting charge recombination (see **Figure 8**a). The interface quality is critical to dictate the electronic properties of the device.[235,236] In a first example,[237] the formation of CuO phase is demonstrated to be detrimental at the ZnO/Cu_2O interface. By removing the CuO phase at the depletion region, V_{oc} increases from ≈110 to 530 mV. In fact, the presence of CuO induces a strong shift (0.4 eV) in the valence band offset between Cu_2O and ZnO, which severely affects V_{oc}. In another study,[183] an aluminum doped ZnO(AZO)/Cu_2O interface is investigated (Figure 8b–d). Buonassisi and co-workers demonstrated that an ultrathin (≈5 nm) transparent amorphous zinc tin oxide (a-ZTO) film efficiently acts as an electron-blocking layer to inhibit charge recombination at the AZO/Cu_2O interface. Electrical measurements indicate that the a-ZTO layer introduces

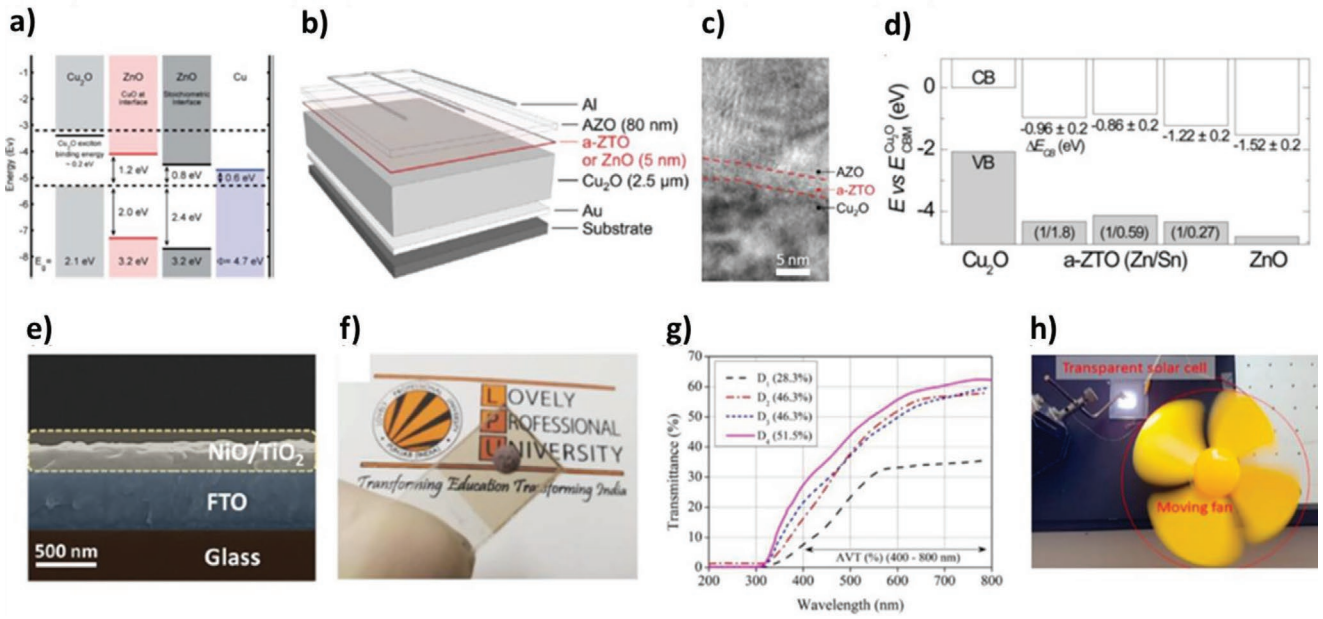

Figure 8. a–d) Interface properties of all-oxide p–n junctions. a) Electronic band structure of Cu_2O/ZnO heterointerface, with/without the presence of CuO phase. Reproduced with permission.[237] Copyright 2014, Royal Society of Chemistry. b–d) Solar cell structure, transmission electron microscopy image, and electronic band structure for a Cu_2O/ZnO heterointerface with the addition of a 5 nm thick a-ZTO layer. Reproduced with permission.[183] Copyright 2013, Royal Society of Chemistry. e–h) Semitransparent all-oxide solar cells. e) SEM image illustrating the structure of a NiO/TiO_2 cell. Reproduced with permission.[241] Copyright 2020, Elsevier. f,g) Image and transmittance of a thin film CuO_x/TiO_2 solar cell. h) Operating device powered by a fully transparent NiO/TiO_2 cell. Reproduced with permission.[241] Copyright 2020, Elsevier.

an effective barrier, inhibiting the electrons to move toward the defect-rich interface, where recombination is maximized. Similar process was also identified in a ZnO/Co_3O_4 system.[184] All these results highlight the importance of both the composition of the homo-/heterostructure and the quality of the interface, under the hypothesis that Cu_2O is the best candidate as p-type absorber for all-oxide solar cells.

On the other side, a recent theoretical study[238] identified the reason for the low efficiency in copper oxide-based PV devices: some of the transitions expected to be active for solar light harvesting are dipole forbidden and the fundamental bandgaps of Cu_4O_3 and CuO, which can form during film growth, are indirect gap phases, inefficient for light-to-electric power conversion. For this reason, alternative light absorbers were recently investigated, including Co_3O_4,[239][240] which represents a promising light absorber for such kind of devices, but on the other hand suffers from high criticality given the difficulties associated to cobalt purchase.[3,5,211] At present, however, no high-efficiency solar cells are reported based on Co_3O_4. In Co_3O_4-based systems, the two main limiting parameters are J_{sc} and FF, while decent V_{oc} were obtained.[240] For this reason, it is still unclear which research direction would be more promising to overcome the limited PCE in such kind of devices. In any case, doping and interface modulation demonstrated effective strategies to tune the electronic properties of the devices.

The ability to tune the electronic structure of oxide heterointerfaces disclosed the possibility to modulate the absorption properties of the devices toward the development of all-oxide transparent or semitransparent solar cells. Two main concepts were applied for the purpose: i) either creating a very thin optically active layer, able to absorb only partially the impinging radiation, ii) or applying wide bandgap p–n junctions, which can absorb UV light and are intrinsically transparent in the visible range. An example in the first category[242] includes a device based on a CuO_x thin film deposited on a TiO_2 layer. The overall thickness of the junction is 150 nm. While a thick CuO_x layer would absorb in the visible range, the thin film allows an average transmittance above 50% in the 400–800 nm range (Figure 8f,g). A different strategy includes the application of two wide bandgap semiconductors to form the p–n junction, as, for instance, NiO and TiO_2 (Figure 8e,h).[241] In this configuration, both the MOSs are transparent to visible light, enabling the solar cell to photoconvert only the radiation falling in the UV spectral region, above the energy gap of the two semiconducting oxides. These solutions are important, toward the development of building-integrated photovoltaics. Unfortunately, due to the full transparency in the visible range, such kinds of cells have a very low PCE. When a sensitizing dye was incorporated in the interface of NiO and TiO_2,[243] J_{SC} was roughly doubled and U_{OC} also increased leading to higher PCE at, however, the expense of the transparency, since the dye mainly absorbs in the visible range. For further details on p-type dye-sensitized solar cells (DSSCs), we address the reader to a complete review on the topic.[244]

3.1.3. Photodoping of Doped MOSs Nanocrystals (NCs) for Light Energy Storage

MOS NCs have the potential to combine both light conversion and energy storage in a unique system. Light absorption and charge storage take place within the same material, making this a fundamentally new concept.[245]

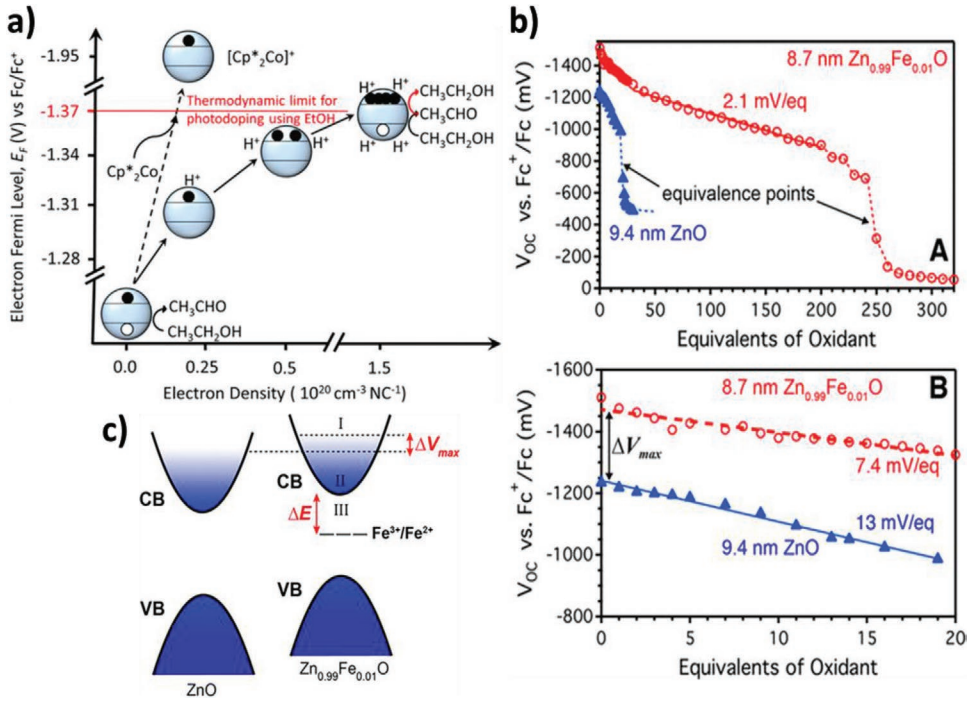

Figure 9. a) Fermi Level variation in ZnO NCs upon photodoping using ethanol as the hole quencher. Reproduced with permission.[246] Copyright 2015, American Chemical Society. b) Potentiometric titration data for undoped and Fe-doped ZnO NCs. c) Band structure of Fe-doped ZnO NCs in comparison with that of undoped ZnO NCs, evidencing the presence of redox-active defects within the bandgap of the former due to the presence of the iron ion dopants. Reproduced with permission.[185] Copyright 2018, American Chemical Society.

The underlying physical process is based on photodoping. Here, the MOS NCs absorb light beyond their bandgap. Similar to the photoconversion process, an electron hole pair is created and the charges are separated at the electronic interface between the NC surface and the surrounding solution. The hole reacts with a sacrificial hole scavenger, such as ethanol, leaving an extra electron in the NC. This process can be repeated by absorbing multiple photons resulting in the storage of hundreds of extra electrons per NCs. The positively charged hole scavenger molecule is electrostatically attracted to the surface of the NC, guaranteeing the overall neutrality of the system and directly affecting the electronic structure of the nanocrystal, resulting in the Fermi level pinning (**Figure 9**a).[246]

The accumulation of electrostatically attracted charge-compensating cations on the negatively photodoped MOS NCs resembles an electric double-layer, as known from supercapacitors. In fact, supercapacitors take advantage of the double-layer electrostatic capacitance in which the separation of the charges over a few angstroms takes place in a double layer at the interface between the charge accumulating species and an electrolyte.[247] Indeed, in MOS NCs, signatures of capacitive and pseudocapacitive charging dynamics were found upon photodoping, indicating that the NCs act as soluble nanosized supercapacitors.[185,248–250] The capacitance of those light driven nanoscale systems has been estimated through the following equation for the double-layer capacitance (C_{dl}) [248]

$$C_{dl} = \frac{A\varepsilon_0\varepsilon_r}{r} \cdot \frac{r+t}{t} \quad (4)$$

with A referring to the sphere's surface area, ε_0 to the permittivity of free space, ε_r to the dielectric constant of the solvent, and r the nanocrystal radius. However, at this point it is not clear which is the dominating mechanism, as in fact a charge transfer at the interface occurs, similar to electrochemical pseudocapacitance.[251]

An experimental way to determine the capacitance is by directly measuring a change in the open-circuit potential (V_{OC}, between the working and counter electrodes) versus charges stored (q). This is obtained with potentiometric titration in which the photoelectrons are counted by introducing molecular oxidants (Figure 9b). From the slope of V_{OC} versus equivalents of titrant, the capacitance C can be extracted, as $C = \Delta q/\Delta V$, where Δq is the change of the charge carriers, and ΔV is the corresponding change in electrochemical potential.[185]

To date photodoping, was mostly shown in indium tin oxide (ITO) NCs, which contains elements that are not earth abundant and hence not highly attractive for integration into energy conversion or storage devices. A significant breakthrough in this field was reached when the photodoping activity of Fe-doped ZnO NCs was demonstrated. This step not only leads to the transition to earth abundant materials but also the choice of dopant impacted considerably on the capacitance. Values in the hundreds of F cm^{-3} and tens of µF cm^{-2} for volumetric and areal capacitance were extracted, respectively,[185] coming close to the performance of commercially available supercapacitor materials.[252,253] The number of extra charges increases significantly following Fe doping. The Fe-dopants introduce acceptor levels with energy just below the conduction band (Figure 9c). After light absorption, the photoinduced electrons reversibly

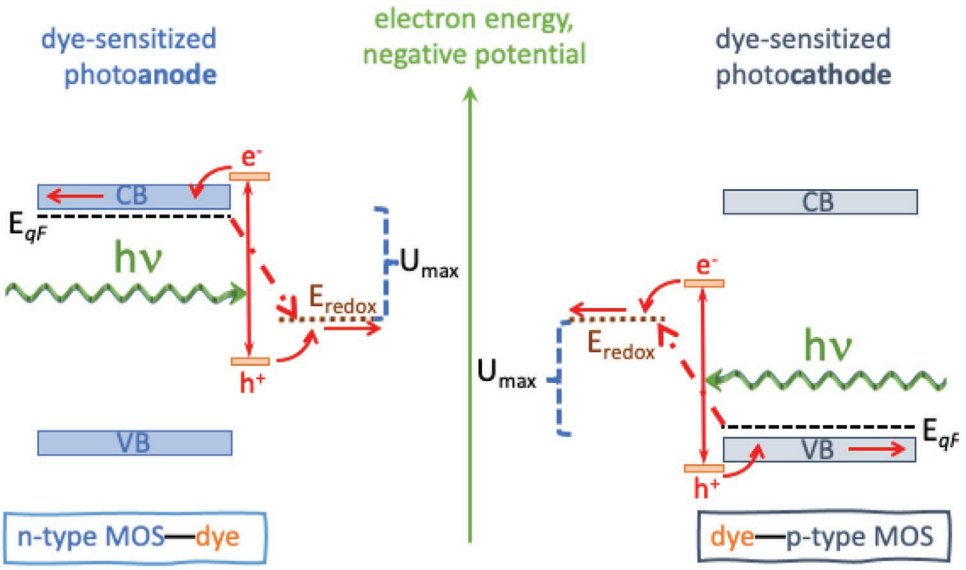

Figure 10. Working principle of MOSs in DSSCs as either photoanode or photocathode. Charge transfer and transport is indicated by red arrows (parasitic recombination dashed–dotted), and the maximum achievable photovoltage U_{max} is shown as the difference of E_{redox} and E_{qF} in the respective case.

relax into these highly localized orbitals and are easily extracted due to the energetic vicinity to the conduction band of the MOS NCs.[185] These results prove that doping control is a promising and viable strategy for the enhancement of charge storage capacity in MOS NCs. They also display the potential of photodoping of optimized doped MOS NCs for light-driven energy storage. However, the exploitation of this process for the next generation of solar energy storage devices still remains a challenge.[254] To exploit the full capability of doped MOS NCs, the process needs to be transferred to fully functional devices that combine light absorption, light conversion, charge storage and redelivery. Photodoping of MOS NCs has the additional potential to merge solar-powered energy storage with multiple charge transfer capability due to the superior stability offered by the delocalization of the stored charges.[255] Merging all these properties into one opens a horizon for novel cost-effective light-driven energy storage devices based on largely abundant MOSs.

3.2. Doped MOSs as Ancillary Materials in Light Harvesting Technologies

3.2.1. Role of Doped MOSs in Dye-Sensitized and Perovskite Solar Cells

Chemically most inert MOSs are often characterized by a band gap energy (E_g) too large to absorb solar radiation. Aside from strategies to introduce new energy levels and, thereby, decrease the apparent E_g by appropriate doping reactions,[256,257] another well-established strategy consists in adding a separate absorber to the surface of a MOS and take care that injection of charges occurs sufficiently fast to suppress competing recombination reactions. Since intimate contact of an absorber site and a MOS is needed to provide these conditions, intensely absorbing materials are required. Aside from another semiconductor layer optimized for high light absorption and low recombination (such as another MOSs, as discussed previously for AOSCs, or a metal halide perovskite, as discussed later), inorganic pigment particles or organic dyes can serve this purpose as long as they provide high absorption coefficients for the solar spectrum and an appropriate energy of the electronic frontier orbitals to inject an electron into the CB of the MOS as a photoanode or inject a hole into the VB of the MOS as a photocathode in a DSSC (**Figure 10**). Since geminate recombination reactions in the absorber heavily compete with injection of charges into MOSs for inorganic as well as organic pigment particles, only nanoparticles ("quantum dots") have a chance as inorganic absorbers and individually adsorbed (dye) molecules as organic absorbers. In order to reach high absorbance (and, hence, keep chances for efficient solar cells) of the overall material system despite such ultrathin coverage of the MOSs by absorbers, a high MOS surface area is a fundamental prerequisite for these types of solar cells as clearly established in the early work of Grätzel in the 1980s and 1990s.

Therefore, porous MOSs deposited on glass covered by a transparent conductive oxide (TCO) are needed. Concepts for DSSCs using either MOS photoanodes (n-type MOS) or photocathodes (p-type MOS) have been established with, however, significantly higher success of cells based on photoanodes.[258] To regenerate the absorber subsequent to injection of charges into the MOS and to complete the electric circuit of the cell, a redox shuttle in solution (that can in some cases be replaced by a solid hole- or electron conductor) perfectly fits the purpose to infiltrate the porous MOS network and contact the absorber sites. The maximum photovoltage U_{max} that can be reached (at open circuit) is limited by the difference of the quasi-Fermi-energy E_{qF} of the injected majority carriers in the MOS and the redox potential E_{redox} of the redox shuttle used (Figure 10). The measured photovoltage at open circuit U_{oc} and the photocurrent generated are heavily decreased by recombination reactions of already injected charge carriers with the reacted form of the redox shuttle (dashed–dotted lines), typically mediated by

trap states for the injected charges in the bulk or at the surface of the MOS.

Doping of MOSs can serve to improve their suitability as electrode materials in DSSCs by three relevant strategies: i) to influence the position of the band edges and shift the respective band edge away from E_{redox}.; ii) to increase the conductivity of the MOS by an increased concentration and/or mobility of majority carriers in order to provide facile charge transport to the back electrode; iii) to decrease the concentration of trap states in the bulk and in particular at the surface of the MOS, decrease the rate of recombination and hinder E_{qF} from shifting towards E_{redox}. With these goals in mind, however, attention always has to be paid to possible consequences of the doping reactions on the morphology (surface area) of the MOSs and the ability to bind absorbers. In the following, the main strategies are elucidated for prominent examples and consequences for the applicability of DSSCs in a sustainable energy supply are derived.

DSSCs based on photoanodes, predominantly composed of annealed (typically at 450 °C) films of nanoparticulate TiO_2, an earth-abundant and non-critical oxide, represent both the origin of the technology[259] and its present state-of-the-art.[260–262] Other MOSs have also been successfully used as photoanodes, such as ZnO and SnO_2 with at least promising efficiencies.[263,264] In an active interplay with improved matching of redox shuttles[265] and optimized sensitizers,[266] surface modifications and doping reaction of MOSs represent the most promising way towards further improvements of today's established DSSCs,[267] according to the three principal strategies introduced above. Increasing the energy of the CB holds promise of increased U_{oc} (Figure 10) as seen in TiO_2 doped with Zr, Nb, W, other metal cations or fluoride anions.[175–177] The conductivity of TiO_2 could also be increased by doping with Ga or Y.[178] Most of these modifications led to increased efficiencies above those of undoped reference TiO_2, but could not reach the efficiency of state-of-the-art TiO_2 cells, presumably because of undesired consequences on film morphology and surface reactivity, which hindered persistent improvements beyond the state-of-the-art. Treatment of nanoparticulate TiO_2 electrodes with $TiCl_4$, on the other hand, has become a routine procedure to improve necking of the particles, increase the conductivity of the films and passivate surface traps.[268] Coverage of the TiO_2 surface by an ultrathin tunnel barrier of MgO[269] or Al_2O_3[270] could also efficiently block recombination. Despite the fact that TiO_2 photoanodes clearly represent the best functioning cells, alternative MOSs are investigated to provide photoanodes of higher electron mobility/conductivity as needed in applications with highly reversible redox shuttles[271] and/or to reach a more sustainable preparation of cells.

ZnO as a traditional competitor of TiO_2, and perhaps an even less CRM compared to the latter; it is chemically more versatile, leading to the advantage of an easier crystallization from solution close to equilibrium conditions, which allows growth of a large variety of nanostructures and porous thin films with high order even at moderate temperatures, but carrying the disadvantage of easier corrosion and mostly disadvantageous surface reactivity, also asking for specially adopted sensitizers.[272–274] From a semiconductor point of view, ZnO carries the advantage of a considerably higher electron mobility at similar positions of CB and VB.[275] Surface electron traps, however, often lead to a downward shift of the CB energy and of E_{qF}, leading to decreased U_{oc}. Surface modification and doping of ZnO has, therefore mainly been used to suppress surface reactivity, passivate surface traps and to hinder recombination. An extreme solution to this problem consists in the preparation of ZnO particles (core) with a shell of an inert oxide like SiO_2 or Al_2O_3 leading to clearly increased stability[276] but carrying the inherent problem of a decreased conductivity for nanoparticulate electrodes. Even a shell of TiO_2 would cause such problem but proved to work for electrodes of ZnO nanowires subsequently coated with TiO_2 but, given the low surface area, with low photovoltaic efficiency.[277] Many facets of bulk doping have been applied to ZnO in order to lift E_{qF} by an increased CB energy or a decreased recombination rate following the passivation of traps and stabilization of the surface.[267,272] Mg-doping of ZnO had proven useful in photocatalysis as a consequence of a higher CB energy and efficient suppressed recombination.[186] The origin of improvements when used in DSSC photoanodes is less clear. Aside from a suppressed recombination arising from an increased conductivity, an increased accessibility of the surface and an even decreased electron transport at higher Mg-content was stated.[278–280] In this context, nanostructures of ZnO cores covered by a Mg-doped ZnO shell turned out beneficial in providing an increased photovoltage (as consequence of Mg-doping) and maintaining a reasonable photocurrent (as a consequence of the improved conduction along the ZnO core) leading to an overall increased cell efficiency compared to pure ZnO.[281] Studies of B-doped or Co-doped ZnO evidenced increased photocurrents, increased U_{oc} and increased overall cell efficiencies caused by decreased recombination.[187,188] Al-doping of ZnO led to improved photocurrents caused by an ameliorated electron conduction, and an increased amount of anchored dye, but either a decreased U_{oc} because of decreased E_g or an increased U_{oc} as a consequence of blocked recombination.[282–284] Doping of ZnO by Ga led to increased charge carrier concentration in the material and increased (albeit low) cell efficiencies as a consequence of widely preserved U_{oc} and increased photocurrents resulting from a higher roughness of the films.[189] Similarly, doping by Sn led to increased efficiencies as a consequence of changes in particle and film morphology.[190] Recently, researchers even started to include more than one dopant (Ti and Cu) into ZnO and stated specific improvements on film morphology by Ti and on the suppression of recombination by Cu, showing, however, the difficulty to assign individual roles to the dopants.[191] In these examples, photoanodes consisting of ZnO showed relevant improvements in DSSC characteristics following doping reactions. They carry the inherent advantage of preparation options at moderate temperature and in a variety of nanostructured films but, up to now, have not reached any cell performance competitive to DSSCs based on TiO_2.

MOSs like SnO_2,[285] Nb_2O_5, WO_3, and In_2O_3[286] have also been studied as photoanode materials in DSSCs but showed even less promise than ZnO despite a number of doping attempts to overcome problems of low band positions, fast recombination and low conductivity. Further, their availability is lower and the energy input is typically higher. Perhaps inspired by the success of dopant interactions, also stoichiometric

ternary oxides like Zn_2SnO_4, $BaSnO_3$, $SrTiO_3$, $ZnTiO_3$, $MgTiO_3$, $CaTiO_3$, $BaTiO_3$, $MgTi_2O_5$, and Mg_2TiO_4, have been studied as photoanode materials[267] sometimes reaching attractively high U_{oc} but low photocurrents because of nonoptimum film morphology, with the exception of Zn_2SnO_4 and $BaSnO_3$,[287,288] for which about half the efficiency of TiO_2-based DSSCs, similar to those of ZnO-based cells, was reached.

The photocathode materials scenario is still mostly dominated by CRM, with NiO clearly leading the field.[289] In addition, even upon wide variation of preparation conditions, doping reactions with lithium or cobalt, surface modification, sensitizing dyes, and redox shuttles, efficiencies not higher than 2.5% were ever reached, limited mainly by rapid recombination of charge carriers.[290–294] A few reports studied other MOSs like CuO, $CuGaO_2$ (also Mg-doped), $CuCrO_2$, or K^+-doped ZnO, but could not reach any competitive efficiency.[295–298]

Aside from MOSs as photoanode or photocathode, MOSs as underlying TCO deserve attention. A high transparency throughout the visible range and a high electric conductivity is needed in order to allow high light harvesting efficiency and low overall charge transport resistance. $In_{0.9}Sn_{0.1}O_{1.6}$ (ITO) or SnO_2 doped with fluoride (FTO) are mostly used. Since annealing reactions are often needed to condition the porous MOS films, FTO is preferred over ITO because of the thermal sensitivity of the latter, and also because replacing scarce In by more abundant Sn and F is convenient. Replacing FTO by Al-doped ZnO (AZO)[192] can further increase the availability. Also, improved injection into AZO compared to FTO was found at least for ZnO-based DSSCs.[193]

In résumé, DSSCs are suitable in particular for applications under diffuse illumination and at higher than typical test temperatures, making them good candidates for building-integrated photovoltaics and indoor applications.[299] They represent a technology of rather low energy-payback-time.[300] Any progress in cell efficiency at conventional preparation technology can further improve this balance. Doping of MOSs can contribute to this task by increasing the photovoltage and the fill factor of cells, provided, however, that the morphology and light-harvesting efficiency of the present record cells can be maintained. Since a considerable part of the energy invested during cell preparation stems from the TCO-glass and since costs for the TCO-glass represent about 20–25% of the overall costs of the cells,[301] technology changes allowing to reduce the energy input to the TCO at widely maintained cell efficiency can play a similarly important role. Avoiding annealing steps, e.g., allows to use plastic foils rather than glass. Electrodeposition of ZnO films instead of sintering TiO_2 nanoparticulate films follows such approach. To increase the notoriously low efficiency of ZnO-based cells, doping reactions again offer improvements for DSSCs based on photoanodes. The field of photocathodes is far less explored, and present studies do not offer technical solutions yet. Tandem cells based on a combination of both, principally offering cells of significantly higher photovoltage and panchromatic absorption are still far out of sight since the current of photocathodes is so much smaller and the smaller current is limiting the overall current in such cells. Therefore, it can be stated that successful doping of MOSs along the three strategies outlined above can serve to develop photoanode materials of optimum performance, preferably prepared from abundant elements at small energy input and, thereby, act as door-opener for DSSCs into their application as significant contributor to a highly sustainable use of solar energy. On this path, more systematic studies are needed to transfer the many promising singular experiences with doped MOSs into a valid concept of DSSCs based on the present state-of-the-art and, hence, provide real technological progress.

More recent is the shift of attention in the PV field toward PSCs, which can be considered direct descendants of DSSCs, since quite similar preparation techniques and MOSs are used. In PSCs, the dye absorber of DSSCs is substituted by a relatively thick crystalline layer of a metal halide perovskite and a solid hole transporting material (HTM) is employed to extract photogenerated holes, a concept already established in solid-state DSSCs as indicated above. In many PSC concepts, MOSs are used as electron transporting layers (ETLs) and the state-of-the-art PSCs are based on anatase TiO_2, either compact or compact + mesoporous, prepared through high temperature sintering, even if many efforts are addressed at finding low temperature processing methods or completely substitute the layer with small molecules.[302,303] Alternatively to TiO_2, SnO_2 is attracting growing attention in the last years,[304] while ZnO demonstrates some intrinsic limitations related to the relatively basic surface chemistry, that, if not compensated, often leads to decomposition of the perovskite layer during device operation.[305] Some MOSs are emerging for the role of HTM, mostly materials similar to those used for photocathodes in DSSCs (NiO mainly, but also Cu_2O, Co_3O_4, or ternary oxides).[302] Doping strategies have been strenuously applied to both MOS-based HTMs and ETLs, to improve the electrical performance of PSCs, particularly in terms of minimized hysteresis and suppressed charge recombination at interfaces. Various elements have been selected as dopant, mostly alkaline or alkaline earth metals (Li, Mg, Cs) but also others relatively abundant such as Zn or Cu, as recently discussed in a detailed review.[302]

3.2.2. MOSs Doping for Spectral Conversion

One of the main issues limiting the efficiency of solar cells is the mismatch between the incident solar spectrum and the cell's spectral response. For instance, for silicon solar cells, which are the most common commercial solar cells covering about 95% share of production in 2019,[306] the record efficiency is about 26–27% depending on the crystallinity of silicon.[307] With a bandgap of 1.12 eV (corresponding to 1100 nm), the greatest efficiency losses arise from non-absorption of the near infrared (NIR) photons, thermalization of the UV-blue photons and extraction losses. PSCs are regarded as one of the most ideal alternatives to silicon solar cells because of their large light absorption coefficient, high charge carrier mobility, and high conversion efficiency. They have rapidly grown to a 25.5% record efficiency,[55] but also the perovskite sensitizer is limited by its bandgap of 1.55 eV (corresponding to 800 nm).[308] Therefore, about 50% of the whole solar energy, falling above that wavelength, is lost. In general, different technologies can cover specific limited regions of the solar spectrum. For a single junction cell, Shockley and Queisser calculated through a detailed balance model in 1961[234] that the maximum theoretical

efficiency is about 33%. Two approaches can be followed to overcome this limit: the development of novel materials and device architectures for broadening the spectral absorption of the solar radiation like in multijunction solar cells, or the realization of additional complementary layers typically in the front or in the back of the active layer with the optical ability to modify the spectrum of the radiation available for the cell.[309] Novel optical approaches to increase the efficiency of solar cells consists in the use of nanostructures, microlenses, plasmonic effects, surface texturing, optical cavities, and antireflection coatings.[310–313] In this paragraph, we focus on the specific subject of spectral conversion layers and the use of doped MOSs therein. Optimized spectral conversion layers would be a cheap high-gain solution for PV solar cell technologies: they can be tuned and optimized for the spectral response of each technology and they can be easily implemented in the production process at low cost. Recent reviews discuss a list of spectral conversion materials and the resulting efficiency enhancement in solar cell devices.[314–316] The possibility to split the energy of one UV photon in two or more NIR photons, known as down-conversion (DC) or quantum cutting, and the possibility to absorb two or more IR photons for producing one NIR photon, referred as up-conversion (UC), were first suggested by François Auzel in 1966 by exploiting rare earth ions. Trupke et al. demonstrated a maximum theoretical efficiency for a silicon solar cell covered with an ideal DC layer as high as 38.6%,[317] while the application of an ideal UC layer on the backside could result in a maximum efficiency of 47.6%[318] under nonconcentrated sunlight. Moreover, luminescent downshifting (LDS) can also be exploited for shifting the energy of one UV/visible photon to a lower energy in the red/NIR, which is particularly useful for silicon solar cells with their poor responses to UV or blue light. However, unlike UC and DC, LDS will not be able to supersede the Shockley–Queisser limit since no additional photons are generating electron–hole pairs.[319]

As anticipated, most of the studies on DC and UC layers involve materials doped with RE^{3+} ions, thus extremely CRMs. Thanks to the high number of available energy levels and wide distribution, covering the whole UV–vis-NIR spectral range, RE^{3+} ions allow the combination of multiple transitions among them, resulting in the sum (UC) or splitting (DC) of the corresponding photon energies and are up to now almost unreplaceable for this specific aim.[320] Optical transitions in RE^{3+} ions are parity forbidden internal 4f transitions, therefore they are characterized by narrow spectral absorptions, low absorption cross sections and long excited-states lifetimes. Proper sensitization strategies are needed to bypass the absorption inefficiency and a wise choice of the matrix is required to avoid undesired losses like multiphonon relaxations, which would decrease the efficiency of spectral conversion processes. Starting from this latter issue, nonradiative multiphonon relaxations are reduced when RE^{3+} ions are surrounded by a low phonon energy material. The best low phonon energy materials are fluoride crystals ($NaYF_4$ ≈370 cm^{-1}; LaF_3 ≈350 cm^{-1}), compared to some oxide crystals (Al_2O_3 ≈600 cm^{-1}) and glasses (SiO_2 glass ≈1100 cm^{-1}).[321] Crystalline hosts offer the additional advantage of higher solubility, lower clustering, and better spectroscopic properties than glasses for RE^{3+} ions. However, the transparency, workability, versatility and lower cost of glasses is often desirable for applications, especially in the field of spectral conversion layers. An excellent combination of the advantages of both glasses and crystals for optics and photonics is provided by the extensive field of glass-ceramics:[322] nanocomposite materials constituted by nanocrystals embedded in a glass matrix. The nanometric size of the inclusions offer some advantages compared to conventional micrometric phosphors such as minimal backscattering to the source, and reduced internal losses.[323] RE^{3+} ions are typically incorporated in the crystalline phase, with significant optical advantages due to the possibility to control the local vibrational and structural properties. The most popular system seems to be the oxyfluoride glass-ceramics,[324] although innovative transparent glass-ceramics for spectral conversion have also been obtained by employing MOSs such as HfO_2,[168,169,325] ZrO_2,[195,326] TiO_2,[179] SnO_2,[171] NCs embedded in silica. Most of these materials present per se relatively low criticalities.

It should be stressed that severe limitations to the efficiency of spectral conversion layers are due to the weak and spectrally limited absorption cross section of RE^{3+} ions, which makes effective applications still far from commercial outcomes. Indeed, typical UC materials work for specific illumination wavelengths and under concentrated sunlight, depending on a nonlinear process that follows a power law.[316] On the other hand, the efficiency enhancement by DC layers is also limited, due to the weak and narrow RE^{3+} ions absorptions. Therefore, the addition of broadband and efficient sensitizers has emerged as a potential keystone for shifting the paradigm from theory to applications for RE^{3+} doped DC materials. In this context, for example, the use of Ag aggregates seems a very promising option (**Figure 11**a), with a broadband and efficient absorption of the whole UV-blue spectral region producing a significant Yb^{3+} 980 nm NIR emission.[170,327–330] In perspective, this is a powerful solution, considering that Ag ion-exchange is a well-known industrial process used for increasing the material refractive index in the realization of optical waveguides,[331] without affecting the optical quality of the material.[332]

Besides using conversion layers or coatings, the possibility of dispersing spectral conversion phosphors inside mesoporous TiO_2 and ZnO photoelectrodes or the direct doping of these MOs by RE^{3+} ions in DSSCs and PSCs was also explored.[194,315] This approach does not solve the intrinsic limitations described above, but may have the additional optical advantage of increasing the scattering of light in the active layer providing a further improvement of the cell's photon absorption.

As a matter of fact, the use of RE^{3+} ions for spectral conversion is strictly related to their peculiar optical properties that currently cannot be replaced by other materials. Although their consumption for spectral conversion is very limited, since they are just dopants in thin layers, they are CRMs and could become more expensive in the future, with possible supplying risks. Therefore, the use of broadband sensitizers is expected to play a major role in perspective, both solving the discussed technical limitations and significantly improving their efficiency, with the possibility to further reduce the amount of RE-doping in optical materials.

In summary, many different optical approaches based on the use of MOSs have been proposed and investigated in the literature to increase the efficiency of solar cells: on the one hand

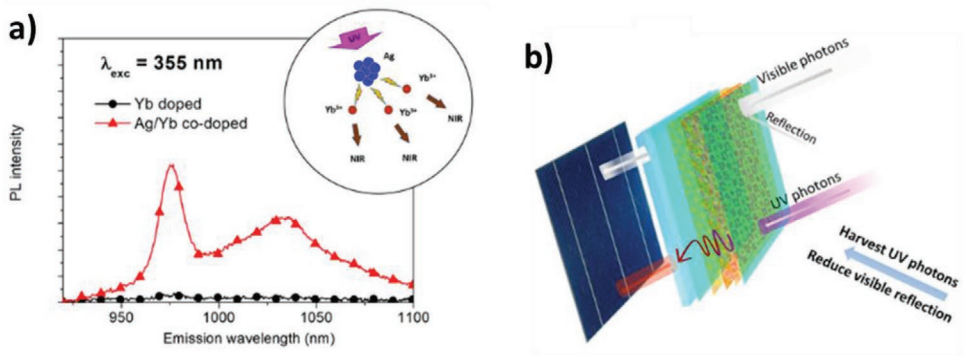

Figure 11. a) Near-infrared photoluminescence emission of Yb3+ doped samples before Ag-exchange and after Ag-exchange. It can be observed that 355 nm is a very weak excitation wavelength for Yb^{3+} ions, while it results in a strong PL emission in Ag-containing samples. Reproduced under the terms of the Creative Common CC BY license.[170] Copyright 2018, the Author(s), Published by MDPI. b) Schematic diagram of the graded-thin-film-coated cover glass interacting with UV and visible photons. Reproduced under the terms of the Creative Commons CC-BY-NC-ND license.[333] Copyright 2021, the Author(s), Published by Elsevier.

by controlling optical phenomena by microlenses, plasmonic structures, texturing, etc; on the other hand, by using spectral conversion materials, mostly based on RE^{3+} ions, to improve the spectral matching between the solar radiation and the cells' response. These approaches revealed strong correlations and sometimes contrasting effects among each other. Therefore, it can be reasonably inferred that, in the not-too-distant future, the best solution will not come from one single approach alone, but it will be obtained by a wise combination of different beneficial contributions. Significant examples are the combination of: i) broadband sensitizers and RE^{3+} ions [170] (Figure 11a); ii) downshifting and scattering when phosphors are dispersed in the DSSCs or PSCs active layer;[194] iii) downshifting coupled to antireflection when phosphors are deposited on the front surface of the cell[333] (Figure 11b); iv) spectral conversion enhanced by plasmonic structures.[334,335]

4. Conclusions and Future Perspectives

In this work, we discussed the role of MOSs in next-generation light-conversion technologies, with particular attention to those based on non-CRM, employing a Janus-faced approach, where the scientific characteristics and socio-economic boundary conditions are inherently linked. Focusing on the former, after proper investigation of the state-of-the-art for the different technologies on a research-scale basis, we provided insights on the potential for integration of non-critical MOSs (i.e., those based on metals such as iron, titanium, zinc, tungsten, copper, and nickel) into technology-relevant devices in particular following optimization of their characteristics by doping. In particular we noted, targeting selectively the use of primary sources of low criticality, that copper oxides will likely have an impact for the further development of AOSCs, titania for PEC and DSSCs, NiO for various hole-transporting ancillary layers in PV, and iron oxides for both PEC and light energy storage. The judicious engineering of these materials (through doping, for example) will ensure to obtain in the next future clean energy from a fully renewable source (the sun), while reducing operation cost of industrial processes (due to the earth-abundance) and fostering sustainability in the long run through the low costs and comparatively lower toxicity with respect to state-of-the-art adopted species. The versatility of their chemistry and chemical reactivity provides a guarantee that a similar optimization will be possible through the current synthetic capabilities that we have available as of today.[336] Synthetic methods are indeed crucial in determining size, composition, crystal structures, dopant/defects level, vacancies, band structures and surface properties and will represent some of the most powerful tools to disclose the full potential of non-critical MOSs for light-conversion applications. In this sense, further interesting perspectives are represented by the use of green chemistry methods, such as the subcritical hydrothermal method or the resorting to biogenic sources,[337–339] to further reduce environmental impacts of energy technologies production lines.

Particular attention was paid to the electronic properties of MOSs that are intrinsically poor due to low mobility of charges. For this reason, we discussed the role of defects (highlighting the thermodynamics of oxygen vacancies) and of dopants that can boost the performance of MOSs and related devices. In order to define the best experimental strategy, a clever design of experiments requires a comprehensive analysis of the interplay between the materials involved, focusing on the quality and the amount of the dopants required (WHO and WHAT in the 5W chart displayed in Figure 4), the chemical environment in which they are located both on a spatial (WHERE) and on a temporal scale (WHEN), and the evaluation of their positive or negative impact on the final properties (WHY). The interplay of these aspects reflects on the choice of the thin-film processing methods and, consequently, on the final structure and morphology/microstructure of the produced MOS layers, that often constitute a real bottleneck for device performance. Consideration of the complex pool of characterization techniques described in Section 2.2 can serve to wisely plan the work so as to achieve the best trade-off in terms of materials/production costs and device efficiency. However, in general, the optimal and proper design of doping conditions is still challenging and complicated: every host lattice has specific requirements (such as geometrical constraints and thermodynamic limitations) that render at present still too difficult to foresee a linear and

straightforward modification strategy. Some promising predictive capabilities are emerging from the use of machine learning approaches in computational materials science and will likely drive the future discovery of proper dopants for selected non-critical MOSs in order to tune their photoconversion performance in the different discussed field.[340–343]

The term "doping" referred here has not the same meaning used in the well-known silicon-based (and other crystalline semiconductors) technology in which a very low concentration of dopants (e.g., boron or phosphorus) substitute the silicon atoms in the crystal lattice with the goal of increasing the free carrier density of silicon without altering the physicochemical properties of the semiconductor (e.g., lattice, chemical stability, energy bandgap, and carriers mobility). Indeed, doping in MOSs gains a much wider meaning in which, as summarized in Table 2, the addition of dopants in the MO lattice is important not only to increase the density of charge carriers (i.e., improving the conductivity), but it is also useful for tuning other properties such as photosensitivity and thermoelectricity, and for engineering the lattice structures and its interplay with others materials, therefore introducing additional degree of freedom in designing novel energy conversion and storage devices.

Another important difference between standard semiconductors doping and MOSs doping is related to how the dopant elements are introduced in the lattice. In the silicon-based technology, a rough controlled doping is achieved either by a bulk diffusion process or by ion implantation. These two technologies require a postprocessing fabrication step (i.e., epitaxy growth) in order to finely control the doping profiles in terms of both concentration and spatial resolution.

However, few aspects can be highlighted. First, the progress in synthetic and characterization capabilities, as discussed above, coupled to the vast knowledge existing as of today in metal ions chemistry, is leading us to achieve a consistent control over substitution also in semiconducting materials with a more chameleonic nature like MOSs.[344][345] Second, both the physical ion implantation and dopant diffusion described above have several drawbacks that a wet chemistry approach in principle does not suffer from: the high energies involved during bombarding may cause alteration of the crystal structure, not only at the surface, but also in the bulk of the material; the high temperatures required during the slow diffusion process are not compatible with MOSs with a low glass transition temperature, and they also increase the technology costs, the coalescence phenomena within the host lattice as well as its environmental impact. In general, these technological issues cause the loss in crystallinity (or symmetry) and thus compromise performances in devices. This is what usually happens when ion implantation is applied to MOSs,[346] that are forced to undergo a further annealing process for restoring a sufficient degree of crystallinity.[347] Furthermore, the complex chemical nature of MOSs implies that, after implantation, the diffusion coefficients of ions are altered by the induced vacancies and interstitials, thus affecting in unpredictable way the performances of devices.[348] Third, assuming that both homovalent and aliovalent chemical ion doping produce impurities,[349] features like strain (and in general mechanical ones[350]), interfacial areas/interface energetics and defects distributions, both in bulk and at interfaces, become extremely relevant and need to be properly investigated when planning the construction of a fully functioning device architectures. It is generally recognized that these features have major effects on physical properties like exciton, charge or ion transport and related studies are attracting increasing interest from the scientific community.[351]

The form in which specific doped MOSs are employed, either as bulk materials or as dimensionally-reduced species like nanoparticles/nanocrystals (0D), nanowires/nanotubes (1D), or layered nanosheets (2D), opens further major issues in functionality control. Thin-film structures fabricated from low-dimensional materials often present complex morphologies and many grain boundaries that can be sources of exciton/charge recombination and thus dramatically affect light-conversion capabilities. On the other hand, the use of nanomaterials offers unique opportunities to tune dopant dislocation,[352–354] defects distribution,[355,356] and energy levels, while also ensuring large surface areas for heterojunctions.[357] Nanostructured films of MOSs are accessible by employing many different techniques, from the most sophisticated ones (because requiring medium to large size and relatively expensive equipment, controlled atmospheres and high energy consumption) like pulse-laser deposition[358], chemical vapor deposition,[359] atomic layer deposition,[360] or magnetron sputtering,[361] up to more common and largely available ones, such as electrochemical methods[362] and various types of solution-processing[363] (dip, spin, and spray coating, printing, and sol–gel methods). In addition, low-dimensional MOSs can be applied as interlayers or as passivating agents to tune interfaces in multilayer bulk architectures. While much has been done in exploring OD and 1D MOS species, the subject of 2D MOSs is only recently emerging at the attention of interdisciplinary research communities,[364] with many interesting discoveries of new materials and properties,[365] such as the reduced Coloumb screening with respect to bulk counterparts, which gives rise to strongly bound excitons, or peculiar electron–phonon coupling profiles. The combination of nanostructuring with tight control over doping will likely pave the way to many more exciting steps ahead in the implementation of doped non-critical MOSs into light-harvesting devices and is suggested by us as a reasonable path to follow for addressing consistent improvements in device performances.

It can be foreseen that the socio-economic impact of a technology will have a steadily growing impact on the materials choices in research and development. In order to increase both sustainability and economic success, industry will continue to adopt for an increasing establishment of (green) energy technologies. Such developments rely on and lead to a corresponding focus in the research in academic institutions and other laboratories of fundamental research. MOS-based technologies exert an undisputed charm for such ongoing and future economic assets because they offer options to use easily accessible and sustainably produced raw materials without the need to excessively worry about their scarcity or negative socio-economic impact. They represent stable materials with relatively low costs of production, since their intrinsic stability allows to use multistep device processing methods where most of the steps do not require the use of an inert atmosphere, vacuum, or a clean room. They generally have low toxicity and allow the use of established green chemistry methods for material synthesis and

processing. Further, durability and stability under typical conditions of applications should not be a major issue. Despite such promising prospects, however, one has to be aware of the fact that initially the devices based on these materials might not have top-notch performance and will need continued optimization.

Based on these considerations, we envision an initial target market for MOSs-based light-harvesting technologies, that could consist of portable/disposable devices, facilitated by a concomitantly established virtuous process of recycling, thus well-fitting to the desired scenario of a fully circular economy framework. The knowledge gained from such implementation within a "niche" market, will allow to design perspectives for the integration of these materials into a large-scale energy conversion scenario. Despite good opportunities for progress in the field can be triggered by decisions in research policy and funding agencies, such perspective ultimately asks for industrial players to reason on the opportunities here discussed, since step-changes in the use of raw materials and manufacturing methods cannot arise from decisions of political entities, but need technology input and should, therefore, be seen as a real chance to reinforce market competitiveness on a global scale. Establishment of production lines for MOS-based light conversion materials and devices will indeed be fully compatible with technologies of new MOS-based energy storage devices for, e.g., e-mobility, and the development of both technologies could benefit from mutual interactions at the research, development, fabrication, and commercialization levels.

Acknowledgements

T.G. and F.L. contributed equally to this work. T.G. and I.K. acknowledge funding from the European Commission through the H2020 FET-PROACTIVE-EIC-07-2020 project "Multi-electron processes for light driven electrodes and electrolytes in conversion and storage of solar energy – LIGHT-CAP" (Project No. 101017821). T.G. also thanks the Verband der Chemischen Industrie e.V. for financial support through the "Fonds der Chemischen Industrie". T.G., D.S., and S.G. acknowledge financial support by Deutsche Forschungsgemeinschaft (DFG) within the RTG (GrK) 2204 "Substitute Materials for Sustainable Energy Technologies." S.G. additionally thanks DFG for a Mercator Fellow position at KIT funded by the DFG within the SFB 1441 – Project-ID 426888090 and DAAD (Germany) for a visiting professorship at JLU. I.K. acknowledges funding from the European Research Council Grant Agreement No. [850875] (Light-DYNAMO). F.L., E.D.M., G.M., and S.G. acknowledge the Interdepartmental Centre Giorgio Levi Cases for Energy Economics and Technology of the University of Padova for the funding of the project AMON-RA. A.V. acknowledges the Kempe Foundation and the Knut & Alice Wallenberg Foundation for financial support.

Conflict of Interest

The authors declare no conflict of interest.

Keywords

critical raw materials, doping, light conversion, metal oxides, semiconductors, sustainable technologies

Received: April 1, 2021
Revised: May 17, 2021
Published online: July 2, 2021

[1] European Commission, European Green Deal (COM/2019/640 Final), **2019**.
[2] "https://ec.europa.eu/info/research-and-innovation/research-area/industrial-research-and-innovation/key-enabling-technologies," (accessed: April 2021).
[3] M. Hofmann, H. Hofmann, C. Hagelüken, A. Hool, *Sustainable Mater. Technol.* **2018**, *17*, e00074.
[4] European Commission, Critical Raw Materials and the Circular Economy – Background Report, **2017**.
[5] European Commission, Critical Raw Materials for Strategic Technologies and Sectors in the EU – a Foresight Study, **2020**.
[6] A. Zuser, H. Rechberger, *Resour., Conserv. Recycl.* **2011**, *56*, 56.
[7] C. Yuan, H. Bin Wu, Y. Xie, X. W. (David) Lou, *Angew. Chem., Int. Ed.* **2014**, *53*, 1488.
[8] F. Wang, Y. Zhang, N. Yu, L. Fu, Y. Zhu, Y. Wu, T. van Ree, in *Metal Oxides in Energy Technologies* (Ed: Y. Wu), Elsevier, New York **2018**, pp. 127–167.
[9] Y. Tretyakov, E. A. Goodilin, *Phys. B: Condens. Matter* **2002**, *321*, 249.
[10] L. Ji, in *Metal Oxides in Energy Technologies* (Ed: Y. Wu), Elsevier, New York **2018**, pp. 49–72.
[11] K. Uchino, in *Metal Oxides in Energy Technologies* (Ed: Y. Wu), Elsevier, New York **2018**, pp. 91–126.
[12] P. Wang, J. Wang, L. Fu, Y. Wu, T. van Ree, in *Metal Oxides in Energy Technologies* (Ed: Y. Wu), Elsevier, New York **2018**, pp. 17–47.
[13] Y. Wang, B. Chen, Y. Zhu, L. Fu, Y. Wu, T. van Ree, in *Metal Oxides in Energy Technologies* (Ed: Y. Wu), Elsevier, New York **2018**, pp. 341–360.
[14] J. Levy, *Phys. Status Solidi* **2002**, *233*, 467.
[15] R. Wang, Y. Jin, B. Xia, H. Xu, *J. Phys. Chem. Lett.* **2020**, *11*, 4036.
[16] M. J. (Mariska) de Wild-Scholten, *Sol. Energy Mater. Sol. Cells* **2013**, *119*, 296.
[17] M. A. Green, *Nat. Energy* **2016**, *1*, 15015.
[18] European Commission, Report on Critical Raw Materials in the Circular Economy, **2018**.
[19] OECD, *OECD Due Diligence Guidance for Responsible Supply Chains of Minerals from Conflict-Affected and High-Risk Areas: Third Edition*, OECD,Paris **2016**.
[20] H. Hofmann, M. C. Schleper, C. Blome, *J. Bus. Ethics* **2018**, *147*, 115.
[21] European Commission, Critical Raw Materials Resilience: Charting a Path towards Greater Security and Sustainability, **2020**.
[22] European Commission, Study on the EU's List of Critical Raw Materials – Final Report, **2020**.
[23] European Commission, EIP on Raw Materials, Raw Materials Scoreboard, **2018**.
[24] K. M. Goodenough, J. Schilling, E. Jonsson, P. Kalvig, N. Charles, J. Tuduri, E. A. Deady, M. Sadeghi, H. Schiellerup, A. Müller, G. Bertrand, N. Arvanitidis, D. G. Eliopoulos, R. A. Shaw, K. Thrane, N. Keulen, *Ore Geol. Rev.* **2016**, *72*, 838.
[25] I. Spanopoulos, W. Ke, M. G. Kanatzidis, *Helv. Chim. Acta* **2021**, *104*, e2000173.
[26] M. Kim, A. Alfano, G. Perotto, M. Serri, N. Dengo, A. Mezzetti, S. Gross, M. Prato, M. Salerno, A. Rizzo, R. Sorrentino, E. Cescon, G. Meneghesso, F. Di Fonzo, A. Petrozza, T. Gatti, F. Lamberti, *Commun. Mater.* **2021**, *2*, 6.
[27] J. Wang, Y. Liu, X. Chen, C. Chen, P. Chen, Z. Wang, Y. Duan, *ChemPhysChem* **2019**, *20*, 2580.
[28] W. C. H. Choy, D. Zhang, *Small* **2016**, *12*, 416.
[29] B. L. Ellis, P. Knauth, T. Djenizian, *Adv. Mater.* **2014**, *26*, 3368.
[30] A. M. Abakumov, S. S. Fedotov, E. V Antipov, J.-M. Tarascon, *Nat. Commun.* **2020**, *11*, 4976.
[31] S. Charoenphon, A. Boonchun, D. Jarukanont, J. T-Thienprasert, P. Reunchan, *RSC Adv.* **2020**, *10*, 19648.
[32] C. A. Cadigan, A. R. Corpuz, F. Lin, C. M. Caskey, K. B. H. Finch, X. Wang, R. M. Richards, *Catal. Sci. Technol.* **2013**, *3*, 900.

[33] O. M. Sousa, J. S. Lima, A. F. Lima, M. V. Lalic, *J. Magn. Magn. Mater.* **2019**, *484*, 21.
[34] R. Aso, D. Kan, Y. Shimakawa, H. Kurata, *Sci. Rep.* **2013**, *3*, 2214.
[35] H. Sartaj Aziz, R. Ali Khan, F. Shah, B. Ismail, J. Nisar, S. Mujtaba Shah, A. Rahim, A. Rahman Khan, *Mater. Sci. Eng. B* **2019**, *243*, 47.
[36] J. Liu, L. Jin, Z. Jiang, L. Liu, L. Himanen, J. Wei, N. Zhang, D. Wang, C.-L. Jia, *J. Chem. Phys.* **2018**, *149*, 244122.
[37] A. Walsh, K. T. Butler, *Acc. Chem. Res.* **2014**, *47*, 364.
[38] J. D. Gale, A. L. Rohl, *Mol. Simul.* **2003**, *29*, 291.
[39] S. E. Derenzo, M. K. Klintenberg, M. J. Weber, *J. Chem. Phys.* **2000**, *112*, 2074.
[40] D. Argyriou, C. Howard, *Aust. J. Phys.* **1992**, *45*, 239.
[41] S. D. Lounis, E. L. Runnerstrom, A. Llordés, D. J. Milliron, *J. Phys. Chem. Lett.* **2014**, *5*, 1564.
[42] D. Smyth, *Solid State Ionics* **2000**, *129*, 5.
[43] S. Aggarwal, R. Ramesh, *Annu. Rev. Mater. Sci.* **1998**, *28*, 463.
[44] *Defects at Oxide Surfaces* (Eds: J. Jupille, G. Thornton), Springer International Publishing, Cham **2015**.
[45] H. L. Tuller, S. R. Bishop, *Annu. Rev. Mater. Res.* **2011**, *41*, 369.
[46] P. Kofstad, *Oxid. Met.* **1995**, *44*, 3.
[47] F. Gunkel, D. V Christensen, Y. Z. Chen, N. Pryds, *Appl. Phys. Lett.* **2020**, *116*, 120505.
[48] K. Ellmer, A. Bikowski, *J. Phys. D. Appl. Phys.* **2016**, *49*, 413002.
[49] J. A. Dawson, Y. Guo, J. Robertson, *Appl. Phys. Lett.* **2015**, *107*, 122110.
[50] J. Zhang, S. Eslava, *Sustainable Energy Fuels* **2019**, *3*, 1351.
[51] C. Di Valentin, G. Pacchioni, *Acc. Chem. Res.* **2014**, *47*, 3233.
[52] J. Robertson, S. J. Clark, *Phys. Rev. B* **2011**, *83*, 075205.
[53] W. Ouyang, F. Teng, J.-H. He, X. Fang, *Adv. Funct. Mater.* **2019**, *29*, 1807672.
[54] V. M. Goldschmidt, *Naturwissenschaften* **1926**, *14*, 477.
[55] https://www.nrel.gov/pv/cell-efficiency.html, "NREL Webpage," (accessed: April 2021).
[56] M. Righetto, D. Meggiolaro, A. Rizzo, R. Sorrentino, Z. He, G. Meneghesso, T. C. Sum, T. Gatti, F. Lamberti, *Prog. Mater. Sci.* **2020**, *110*, 100639.
[57] C. J. Bartel, C. Sutton, B. R. Goldsmith, R. Ouyang, C. B. Musgrave, L. M. Ghiringhelli, M. Scheffler, *Sci. Adv.* **2019**, *5*, eaav0693.
[58] S. Vasala, M. Karppinen, *Prog. Solid State Chem.* **2015**, *43*, 1.
[59] P.-K. Kung, M.-H. Li, P.-Y. Lin, J.-Y. Jhang, M. Pantaler, D. C. Lupascu, G. Grancini, P. Chen, *Sol. RRL* **2020**, *4*, 1900306.
[60] A. Kumar, A. S. Verma, S. R. Bhardwaj, *Open Appl. Phys. J.* **2008**, *1*, 11.
[61] X. Liu, S. Li, Z. Li, Y. Zhang, W. Yang, Z. Li, H. Liu, D. V. Shtansky, X. Fang, *Adv. Funct. Mater.* **2021**, *31*, 2101480.
[62] A. Othonos, C. Christofides, M. Zervos, *Appl. Phys. Lett.* **2013**, *103*, 133112.
[63] J. Buckeridge, C. R. A. Catlow, M. R. Farrow, A. J. Logsdail, D. O. Scanlon, T. W. Keal, P. Sherwood, S. M. Woodley, A. A. Sokol, A. Walsh, *Phys. Rev. Mater.* **2018**, *2*, 054604.
[64] W. Khan, A. H. Naqvi, M. Gupta, S. Husain, R. Kumar, *J. Chem. Phys.* **2011**, *135*, 054501.
[65] S. Baranovski, O. Rubel, *Charge Transport in Disordered Solids with Applications in Electronics*, John Wiley & Sons, Ltd, Chichester **2006**, pp. 49–96.
[66] A. Banerjee, S. Pal, B. K. Chaudhuri, *J. Chem. Phys.* **2001**, *115*, 1550.
[67] M. A. Lampert, *Phys. Rev.* **1956**, *103*, 1648.
[68] H.-J. Chung, J. H. Jeong, T. K. Ahn, H. J. Lee, M. Kim, K. Jun, J.-S. Park, J. K. Jeong, Y.-G. Mo, H. D. Kim, *Electrochem. Solid-State Lett.* **2008**, *11*, H51.
[69] M. D. Purkayastha, S. Middya, J. Datta, P. P. Ray, B. D. Biswas, M. Sarkar, G. K. Darbha, N. Singh, T. P. Majumder, P. Saha, D. Das, *Mater. Chem. Phys.* **2019**, *226*, 362.
[70] D. Shi, V. Adinolfi, R. Comin, M. Yuan, E. Alarousu, A. Buin, Y. Chen, S. Hoogland, A. Rothenberger, K. Katsiev, Y. Losovyj, X. Zhang, P. A. Dowben, O. F. Mohammed, E. H. Sargent, O. M. Bakr, *Science* **2015**, *347*, 519.
[71] H. von D. Briggs, *Phys. Unserer Zeit* **1979**, *10*, 30.
[72] M. N. Islam, T. B. Ghosh, K. L. Chopra, H. N. Acharya, *Thin Solid Films* **1996**, *280*, 20.
[73] M.-H. Park, J.-H. Li, A. Kumar, G. Li, Y. Yang, *Adv. Funct. Mater.* **2009**, *19*, 1241.
[74] S.-S. Li, Y.-K. Su, *RSC Adv.* **2019**, *9*, 2941.
[75] P. Dalle Feste, M. Crisci, F. Barbon, F. Tajoli, M. Salerno, F. Drago, M. Prato, S. Gross, T. Gatti, F. Lamberti, *Appl. Sci.* **2021**, *11*, 2016.
[76] K. Dyrek, M. Che, *Chem. Rev.* **1997**, *97*, 305.
[77] A. Gulino, I. Fragala, *Chem. Mater.* **2002**, *14*, 116.
[78] D. A. Zatsepin, D. W. Boukhvalov, E. Z. Kurmaev, I. S. Zhidkov, S. S. Kim, L. Cui, N. V. Gavrilov, S. O. Cholakh, *Phys. Status Solidi* **2015**, *252*, 1890.
[79] B. K. Teo, *EXAFS: Basic Principles and Data Analysis*, Springer Berlin Heidelberg, Berlin **1986**.
[80] A. Kuzmin, J. Chaboy, *IUCrJ* **2014**, *1*, 571.
[81] F. Haass, T. Buhrmester, M. Martin, *Phys. Chem. Chem. Phys.* **2001**, *3*, 4806.
[82] S. Kumar, C. E. Graves, J. P. Strachan, E. M. Grafals, A. L. D. Kilcoyne, T. Tyliszczak, J. N. Weker, Y. Nishi, R. S. Williams, *Adv. Mater.* **2016**, *28*, 2772.
[83] D.-H. Ha, L. M. Moreau, S. Honrao, R. G. Hennig, R. D. Robinson, *J. Phys. Chem. C* **2013**, *117*, 14303.
[84] M. Niedermaier, T. Schwab, P. Dolcet, J. Bernardi, S. Gross, M. Bockstedte, O. Diwald, *J. Phys. Chem. C* **2019**, *123*, 25991.
[85] A. I. Becerro, M. Allix, M. Laguna, D. González-Mancebo, C. Genevois, A. Caballero, G. Lozano, N. O. Núñez, M. Ocaña, *J. Mater. Chem. C* **2018**, *6*, 12830.
[86] S.-H. Liao, H.-J. Jhuo, P.-N. Yeh, Y.-S. Cheng, Y.-L. Li, Y.-H. Lee, S. Sharma, S.-A. Chen, *Sci. Rep.* **2015**, *4*, 6813.
[87] L. B. McCusker, R. B. Von Dreele, D. E. Cox, D. Louër, P. Scardi, *J. Appl. Crystallogr.* **1999**, *32*, 36.
[88] H. M. Rietveld, *J. Appl. Crystallogr.* **1969**, *2*, 65.
[89] M. Leoni, R. Maggio, S. Polizzi, P. Scardi, *J. Am. Ceram. Soc.* **2004**, *87*, 1133.
[90] C. Malerba, C. L. Azanza Ricardo, M. D'Incau, F. Biccari, P. Scardi, A. Mittiga, *Sol. Energy Mater. Sol. Cells* **2012**, *105*, 192.
[91] K. C. Verma, R. K. Kotnala, *Phys. Chem. Chem. Phys.* **2016**, *18*, 5647.
[92] A. B. Habtemariam, D. M. Kabtamu, M. Maaza, *SN Appl. Sci.* **2019**, *1*, 413.
[93] A. Paone, R. Sanjines, P. Jeanneret, H. J. Whitlow, E. Guibert, G. Guibert, F. Bussy, J.-L. Scartezzini, A. Schüler, *J. Alloys Compd.* **2015**, *621*, 206.
[94] O. Sakata, M. Nakamura, *Surface Science Techniques*, Springer, Berlin **2013**, pp. 165–190.
[95] P. van der Heide, *Secondary Ion Mass Spectrometry*, John Wiley & Sons, Inc., Hoboken, NJ **2014**.
[96] *Materials Characterization*, ASM International, Novelty, OH **2019**, pp. 173–184.
[97] U. N. Gries, H. Schraknepper, K. Skaja, F. Gunkel, S. Hoffmann-Eifert, R. Waser, R. A. De Souza, *Phys. Chem. Chem. Phys.* **2018**, *20*, 989.
[98] D. Barreca, G. Carraro, A. Gasparotto, C. Maccato, M. E. A. Warwick, E. Toniato, V. Gombac, C. Sada, S. Turner, G. Van Tendeloo, P. Fornasiero, *Adv. Mater. Interfaces* **2016**, *3*, 1600348.
[99] A. Gasparotto, C. Maccato, G. Carraro, C. Sada, U. L. Štangar, B. Alessi, C. Rocks, D. Mariotti, A. La Porta, T. Altantzis, D. Barreca, *ACS Appl. Mater. Interfaces* **2019**, *11*, 15881.
[100] C. Liu, F. Yun, B. Xiao, S.-J. Cho, Y. T. Moon, H. Morkoç, M. Abouzaid, R. Ruterana, K. M. Yu, W. Walukiewicz, *J. Appl. Phys.* **2005**, *97*, 126107.
[101] S. Das, T. L. Alford, *J. Appl. Phys.* **2013**, *113*, 244905.
[102] W. Zhou, I. E. Wachs, C. J. Kiely, *Curr. Opin. Solid State Mater. Sci.* **2012**, *16*, 10.

[103] M. Kitta, N. Taguchi, H. Sudrajat, H. Onishi, *Appl. Phys. Lett.* **2021**, *118*, 153901.
[104] M. D. Rossell, Q. M. Ramasse, S. D. Findlay, F. Rechberger, R. Erni, M. Niederberger, *ACS Nano* **2012**, *6*, 7077.
[105] Y. Li, X.-P. Wu, N. Jiang, M. Lin, L. Shen, H. Sun, Y. Wang, M. Wang, X. Ke, Z. Yu, F. Gao, L. Dong, X. Guo, W. Hou, W. Ding, X.-Q. Gong, C. P. Grey, L. Peng, *Nat. Commun.* **2017**, *8*, 581.
[106] J. V. Hanna, M. E. Smith, *Solid State Nucl. Magn. Reson.* **2010**, *38*, 1.
[107] P. G. Bruce, B. Scrosati, J.-M. Tarascon, *Angew. Chem., Int. Ed.* **2008**, *47*, 2930.
[108] M. Wang, X.-P. Wu, S. Zheng, L. Zhao, L. Li, L. Shen, Y. Gao, N. Xue, X. Guo, W. Huang, Z. Gan, F. Blanc, Z. Yu, X. Ke, W. Ding, X.-Q. Gong, C. P. Grey, L. Peng, *Sci. Adv.* **2015**, *1*, e1400133.
[109] T. Tsubota, M. Ohtaki, K. Eguchi, H. Arai, *J. Mater. Chem.* **1997**, *7*, 85.
[110] Y. S. Avadhut, J. Weber, E. Hammarberg, C. Feldmann, I. Schellenberg, R. Pöttgen, J. Schmedt auf der Günne, *Chem. Mater.* **2011**, *23*, 1526.
[111] S. Corby, L. Francàs, A. Kafizas, J. R. Durrant, *Chem. Sci.* **2020**, *11*, 2907.
[112] S. Sorenson, E. Driscoll, S. Haghighat, J. M. Dawlaty, *J. Phys. Chem. C* **2014**, *118*, 23621.
[113] M. E. Vaida, S. R. Leone, *J. Phys. Chem. C* **2016**, *120*, 2769.
[114] S. Selim, E. Pastor, M. García-Tecedor, M. R. Morris, L. Francàs, M. Sachs, B. Moss, S. Corby, C. A. Mesa, S. Gimenez, A. Kafizas, A. A. Bakulin, J. R. Durrant, *J. Am. Chem. Soc.* **2019**, *141*, 18791.
[115] R. Fernández-Climent, S. Giménez, M. García-Tecedor, *Sustainable Energy Fuels* **2020**, *4*, 5916.
[116] A. J. E. Rettie, W. D. Chemelewski, D. Emin, C. B. Mullins, *J. Phys. Chem. Lett.* **2016**, *7*, 471.
[117] S. R. Pendlebury, M. Barroso, A. J. Cowan, K. Sivula, J. Tang, M. Grätzel, D. Klug, J. R. Durrant, *Chem. Commun.* **2011**, *47*, 716.
[118] H. G. Baldoví, B. Ferrer, M. Álvaro, H. García, *J. Phys. Chem. C* **2014**, *118*, 9275.
[119] F. Teng, K. Hu, W. Ouyang, X. Fang, *Adv. Mater.* **2018**, *30*, 1706262.
[120] W. Shockley, W. T. Read, *Phys. Rev.* **1952**, *87*, 835.
[121] D. Bisi, M. Meneghini, C. de Santi, A. Chini, M. Dammann, P. Bruckner, M. Mikulla, G. Meneghesso, E. Zanoni, *IEEE Trans. Electron Devices* **2013**, *60*, 3166.
[122] N. Lago, A. Cester, N. Wrachien, E. Benvenuti, S. D. Quiroga, M. Natali, S. Toffanin, M. Muccini, G. Meneghesso, *IEEE Trans. Electron Devices* **2016**, *63*, 4432.
[123] T. P. Nguyen, J. Ip, O. Gaudin, R. B. Jackman, *Eur. Phys. J. Appl. Phys.* **2004**, *27*, 219.
[124] A. Chasin, E. Simoen, A. Bhoolokam, M. Nag, J. Genoe, G. Gielen, P. Heremans, *Appl. Phys. Lett.* **2014**, *104*, 082112.
[125] V. K. Tewary, S. C. Jain, *Adv. Electron. Electr. Phys.* **1986**, *67*, 329.
[126] P. Lopez-Varo, J. A. Jiménez-Tejada, M. García-Rosell, S. Ravishankar, G. Garcia-Belmonte, J. Bisquert, O. Almora, *Adv. Energy Mater.* **2018**, *8*, 1702772.
[127] B. C. O'Regan, P. R. F. Barnes, X. Li, C. Law, E. Palomares, J. M. Marin-Beloqui, *J. Am. Chem. Soc.* **2015**, *137*, 5087.
[128] S. Ravishankar, S. Gharibzadeh, C. Roldán-Carmona, G. Grancini, Y. Lee, M. Ralaiarisoa, A. M. Asiri, N. Koch, J. Bisquert, M. K. Nazeeruddin, *Joule* **2018**, *2*, 788.
[129] A. R. C. Bredar, A. L. Chown, A. R. Burton, B. H. Farnum, *ACS Appl. Energy Mater.* **2020**, *3*, 66.
[130] E. Thimsen, S. Biswas, C. S. Lo, P. Biswas, *J. Phys. Chem. C* **2009**, *113*, 2014.
[131] B. Tandon, S. Ghosh, D. J. Milliron, *Chem. Mater.* **2019**, *31*, 7752.
[132] R. Buonsanti, D. J. Milliron, *Chem. Mater.* **2013**, *25*, 1305.
[133] A. Agrawal, S. H. Cho, O. Zandi, S. Ghosh, R. W. Johns, D. J. Milliron, *Chem. Rev.* **2018**, *118*, 3121.
[134] A. Klein, C. Körber, A. Wachau, F. Säuberlich, Y. Gassenbauer, S. P. Harvey, D. E. Proffit, T. O. Mason, *Materials* **2010**, *3*, 4892.
[135] M. Kröger, S. Hamwi, J. Meyer, T. Riedl, W. Kowalsky, A. Kahn, *Org. Electron.* **2009**, *10*, 932.
[136] C. Maragliano, S. Lilliu, M. S. Dahlem, M. Chiesa, T. Souier, M. Stefancich, *Sci. Rep.* **2015**, *4*, 4203.
[137] M. Kumar, S. Mookerjee, T. Som, *Nanotechnology* **2016**, *27*, 375702.
[138] M. Nolan, S. D. Elliott, J. S. Mulley, R. A. Bennett, M. Basham, P. Mulheran, *Phys. Rev. B* **2008**, *77*, 235424.
[139] R. Gottesman, I. Levine, M. Schleuning, R. Irani, D. Abou-Ras, T. Dittrich, D. Friedrich, R. Krol, *Adv. Energy Mater.* **2021**, *11*, 2003474.
[140] D. Kang, N. Park, *Adv. Mater.* **2019**, *31*, 1805214.
[141] A. Rizzo, F. Lamberti, M. Buonomo, N. Wrachien, L. Torto, N. Lago, S. Sansoni, R. Pilot, M. Prato, N. Michieli, M. Meneghetti, G. Meneghesso, A. Cester, *Sol. Energy Mater. Sol. Cells* **2019**, *189*, 43.
[142] M. Sajedi Alvar, P. W. M. Blom, G.-J. A. H. Wetzelaer, *Nat. Commun.* **2020**, *11*, 4023.
[143] D. C. Jordan, T. J. Silverman, J. H. Wohlgemuth, S. R. Kurtz, K. T. VanSant, *Prog. Photovoltaics Res. Appl.* **2017**, *25*, 318.
[144] E. von Hauff, *J. Phys. Chem. C* **2019**, *123*, 11329.
[145] V. Balasubramani, S. Chandraleka, T. S. Rao, R. Sasikumar, M. R. Kuppusamy, T. M. Sridhar, *J. Electrochem. Soc.* **2020**, *167*, 037572.
[146] S. Pokhrel, C. E. Simion, V. Quemener, N. Bârsan, U. Weimar, *Sens. Actuators, B* **2008**, *133*, 78.
[147] F. Klein, R. Pinedo, B. B. Berkes, J. Janek, P. Adelhelm, *J. Phys. Chem. C* **2017**, *121*, 8679.
[148] G. Garcia-Belmonte, J. Bisquert, *ACS Energy Lett.* **2016**, *1*, 683.
[149] G. Feher, *Phys. Rev.* **1959**, *114*, 1219.
[150] F. Napoli, M. Chiesa, S. Livraghi, E. Giamello, S. Agnoli, G. Granozzi, G. Pacchioni, C. Di Valentin, *Chem. Phys. Lett.* **2009**, *477*, 135.
[151] M. D'Arienzo, N. Siedl, A. Sternig, R. Scotti, F. Morazzoni, J. Bernardi, O. Diwald, *J. Phys. Chem. C* **2010**, *114*, 18067.
[152] A. Folli, J. Z. Bloh, E.-P. Beukes, R. F. Howe, D. E. Macphee, *J. Phys. Chem. C* **2013**, *117*, 22149.
[153] A. M. Czoska, S. Livraghi, M. C. Paganini, E. Giamello, C. Di Valentin, G. Pacchioni, *Phys. Chem. Chem. Phys.* **2011**, *13*, 136.
[154] A. Guler, L. Arda, N. Dogan, C. Boyraz, E. Ozugurlu, *Ceram. Int.* **2019**, *45*, 1737.
[155] M. A. Marzouk, H. A. ElBatal, A. M. Abdel Ghany, F. M. Ezz Eldin, *J. Mol. Struct.* **2011**, *997*, 94.
[156] R. Wang, A. W. Sleight, D. Cleary, *Chem. Mater.* **1996**, *8*, 433.
[157] I. S. Brandt, M. A. Tumelero, C. A. Martins, C. C. Plá Cid, R. Faccio, A. A. Pasa, *J. Appl. Phys.* **2018**, *123*, 161412.
[158] F. Hu, Y. Zou, L. Wang, Y. Wen, Y. Xiong, *Int. J. Hydrogen Energy* **2016**, *41*, 15172.
[159] M. Zhang, J. Wang, H. Xue, J. Zhang, S. Peng, X. Han, Y. Deng, W. Hu, *Angew. Chem., Int. Ed.* **2020**, *59*, 18463.
[160] Y. C. Lin, L. C. Hsu, C. Y. Lin, C. L. Chiang, C. M. Chou, W. W. Wu, S. Y. Chen, Y. G. Lin, *ACS Appl. Mater. Interfaces* **2019**, *11*, 38625.
[161] D. Monllor-Satoca, M. Bärtsch, C. Fàbrega, A. Genç, S. Reinhard, T. Andreu, J. Arbiol, M. Niederberger, J. R. Morante, *Energy Environ. Sci.* **2015**, *8*, 3242.
[162] Z. Zhang, I. Karimata, H. Nagashima, S. Muto, K. Ohara, K. Sugimoto, T. Tachikawa, *Nat. Commun.* **2019**, *10*, 4832.
[163] R. Mazzaro, S. Boscolo Bibi, M. Natali, G. Bergamini, V. Morandi, P. Ceroni, A. Vomiero, *Nano Energy* **2019**, *61*, 36.
[164] J. Y. Kim, G. Magesh, D. H. Youn, J. W. Jang, J. Kubota, K. Domen, J. S. Lee, *Sci. Rep.* **2013**, *3*, 2681.
[165] A. Kay, I. Cesar, M. Grätzel, *J. Am. Chem. Soc.* **2006**, *128*, 15714.
[166] M. Li, Y. Yang, Y. Ling, W. Qiu, F. Wang, T. Liu, Y. Song, X. Liu, P. Fang, Y. Tong, Y. Li, *Nano Lett.* **2017**, *17*, 2490.
[167] K. D. Malviya, H. Dotan, D. Shlenkevich, A. Tsyganok, H. Mor, A. Rothschild, *J. Mater. Chem. A* **2016**, *4*, 3091.

[168] A. Bouajaj, S. Belmokhtar, M. R. Britel, C. Armellini, B. Boulard, F. Belluomo, A. Di Stefano, S. Polizzi, A. Lukowiak, M. Ferrari, F. Enrichi, *Opt. Mater.* **2016**, *52*, 62.
[169] L. Zur, C. Armellini, S. Belmokhtar, A. Bouajaj, E. Cattaruzza, A. Chiappini, F. Coccetti, M. Ferrari, F. Gonella, G. C. Righini, E. Trave, A. Vomiero, F. Enrichi, *Opt. Mater.* **2019**, *87*, 102.
[170] F. Enrichi, E. Cattaruzza, M. Ferrari, F. Gonella, R. Ottini, P. Riello, G. C. Righini, E. Trave, A. Vomiero, L. Zur, *Micromachines* **2018**, *9*, 380.
[171] J. J. Velázquez, A. C. Yanes, J. Del-Castillo, C. Guzmán-Afonso, V. D. Rodríguez, *Sci. Adv. Mater.* **2015**, *7*, 2272.
[172] G. Zhu, T. Lin, H. Cui, W. Zhao, H. Zhang, F. Huang, *ACS Appl. Mater. Interfaces* **2016**, *8*, 122.
[173] C. Di Valentin, G. Pacchioni, *Catal. Today* **2013**, *206*, 12.
[174] X. Chen, L. Liu, P. Y. Yu, S. S. Mao, *Science* **2011**, *331*, 746.
[175] X. Zhang, F. Liu, Q.-L. Huang, G. Zhou, Z.-S. Wang, *J. Phys. Chem. C* **2011**, *115*, 12665.
[176] S. Lee, J. H. Noh, H. S. Han, D. K. Yim, D. H. Kim, J.-K. Lee, J. Y. Kim, H. S. Jung, K. S. Hong, *J. Phys. Chem. C* **2009**, *113*, 6878.
[177] V. Madurai Ramakrishnan, M. Natarajan, S. Pitchaiya, A. Santhanam, D. Velauthapillai, A. Pugazhendhi, *Int. J. Energy Res.* **2020**, 1, https://doi.org/10.1002/er.5882.
[178] A. K. Chandiran, F. Sauvage, L. Etgar, M. Graetzel, *J. Phys. Chem. C* **2011**, *115*, 9232.
[179] J. M. M. Buarque, D. Manzani, S. L. Scarpari, M. Nalin, S. J. L. Ribeiro, J. Esbenshade, M. A. Schiavon, J. L. Ferrari, *Mater. Res. Bull.* **2018**, *107*, 295.
[180] H. Song, Y. Li, Z. Lou, M. Xiao, L. Hu, Z. Ye, L. Zhu, *Appl. Catal., B* **2015**, *112*, 166.
[181] A. Paracchino, V. Laporte, K. Sivula, M. Grätzel, E. Thimsen, *Nat. Mater.* **2011**, *10*, 456.
[182] M. Gaudon, O. Toulemonde, A. Demourgues, *Inorg. Chem.* **2007**, *46*, 10996.
[183] Y. S. Lee, J. Heo, S. C. Siah, J. P. Mailoa, R. E. Brandt, S. B. Kim, R. G. Gordon, T. Buonassisi, *Energy Environ. Sci.* **2013**, *6*, 2112.
[184] P. Ghamgosar, F. Rigoni, M. G. Kohan, S. You, E. A. Morales, R. Mazzaro, V. Morandi, N. Almqvist, I. Concina, A. Vomiero, *ACS Appl. Mater. Interfaces* **2019**, *11*, 23454.
[185] C. K. Brozek, D. Zhou, H. Liu, X. Li, K. R. Kittilstved, D. R. Gamelin, *Nano Lett.* **2018**, *18*, 3297.
[186] X. Qiu, L. Li, J. Zheng, J. Liu, X. Sun, G. Li, *J. Phys. Chem. C* **2008**, *112*, 12242.
[187] K. Mahmood, S. Bin Park, *J. Mater. Chem. A* **2013**, *1*, 4826.
[188] G. Kanimozhi, S. Vinoth, H. Kumar, E. S. Srinadhu, N. Satyanarayana, *Mater. Res. Express* **2018**, *6*, 025041.
[189] A. S. Gonçalves, M. S. Góes, F. Fabregat-Santiago, T. Moehl, M. R. Davolos, J. Bisquert, S. Yanagida, A. F. Nogueira, P. R. Bueno, *Electrochim. Acta* **2011**, *56*, 6503.
[190] S. Ameen, M. S. Akhtar, H.-K. Seo, Y. S. Kim, H. S. Shin, *Chem. Eng. J.* **2012**, *187*, 351.
[191] B. Mehmood, M. I. Khan, M. Iqbal, A. Mahmood, W. Al-Masry, *Int. J. Energy Res.* **2021**, *45*, 2445.
[192] K. H. Kim, K. C. Park, D. Y. Ma, *J. Appl. Phys.* **1997**, *81*, 7764.
[193] S.-H. Lee, S.-H. Han, H. S. Jung, H. Shin, J. Lee, J.-H. Noh, S. Lee, I.-S. Cho, J.-K. Lee, J. Kim, H. Shin, *J. Phys. Chem. C* **2010**, *114*, 7185.
[194] S. K. Karunakaran, G. M. Arumugam, W. Yang, S. Ge, S. Khan, X. Lin, G. Yang, *ACS Sustainable Chem. Eng.* **2021**, *9*, 1035.
[195] F. Enrichi, E. Cattaruzza, P. Riello, G. C. Righini, A. Vomiero, *Ceram. Int.* **2021**, *47*, 17939.
[196] W. Yang, R. R. Prabhakar, J. Tan, S. D. Tilley, J. Moon, *Chem. Soc. Rev.* **2019**, *48*, 4979.
[197] K. Sivula, R. van de Krol, *Nat. Rev. Mater.* **2016**, *1*, 15010.
[198] S. J. A. Moniz, S. A. Shevlin, D. J. Martin, Z.-X. Guo, J. Tang, *Energy Environ. Sci.* **2015**, *8*, 731.
[199] I. Roger, M. A. Shipman, M. D. Symes, *Nat. Rev. Chem.* **2017**, *1*, 0003.
[200] J. H. Kim, D. Hansora, P. Sharma, J. W. Jang, J. S. Lee, *Chem. Soc. Rev.* **2019**, *48*, 1908.
[201] S. Lin, H. Huang, T. Ma, Y. Zhang, *Adv. Sci.* **2020**, *2002458*, 23.
[202] C. Xia, H. Wang, J. K. Kim, J. Wang, *Adv. Funct. Mater.* **2020**, *31*, 2008247.
[203] H. Wu, H. L. Tan, C. Y. Toe, J. Scott, L. Wang, R. Amal, Y. H. Ng, *Adv. Mater.* **2020**, *32*, 1904717.
[204] J. Zhang, J. Cui, S. Eslava, *Adv. Energy Mater.* **2021**, *11*, 2003111.
[205] L. Alibabaei, H. Luo, R. L. House, P. G. Hoertz, R. Lopez, T. J. Meyer, *J. Mater. Chem. A* **2013**, *1*, 4133.
[206] G. Rossi, L. Pasquini, D. Catone, A. Piccioni, N. Patelli, A. Paladini, A. Molinari, S. Caramori, P. O'Keeffe, F. Boscherini, *Appl. Catal., B* **2018**, *237*, 603.
[207] X. Wang, L. Mayrhofer, M. Hoefer, S. Estrade, L. Lopez-Conesa, H. Zhou, Y. Lin, F. Peiró, Z. Fan, H. Shen, L. Schaefer, M. Moseler, G. Braeuer, A. Waag, *Adv. Energy Mater.* **2019**, *9*, 1900725.
[208] T. W. Kim, K. S. Choi, *Science* **2014**, *343*, 990.
[209] T. Li, T. Kasahara, J. He, K. E. Dettelbach, G. M. Sammis, C. P. Berlinguette, *Nat. Commun.* **2017**, *8*, 6.
[210] H. G. Cha, K. S. Choi, *Nat. Chem.* **2015**, *7*, 328.
[211] T. E. Graedel, E. M. Harper, N. T. Nassar, P. Nuss, B. K. Reck, B. L. Turner, *Proc. Natl. Acad. Sci. USA* **2015**, *112*, 4257.
[212] I. V. Bagal, N. R. Chodankar, M. A. Hassan, A. Waseem, M. A. Johar, D. H. Kim, S. W. Ryu, *Int. J. Hydrogen Energy* **2019**, *44*, 21351.
[213] J. Luo, L. Steier, M. K. Son, M. Schreier, M. T. Mayer, M. Grätzel, *Nano Lett.* **2016**, *16*, 1848.
[214] L. Pan, J. H. Kim, M. T. Mayer, M.-K. Son, A. Ummadisingu, J. S. Lee, A. Hagfeldt, J. Luo, M. Grätzel, *Nat. Catal.* **2018**, *1*, 412.
[215] L. Pan, Y. Liu, L. Yao, Dan Ren, K. Sivula, M. Grätzel, A. Hagfeldt, D. Ren, K. Sivula, M. Grätzel, A. Hagfeldt, *Nat. Commun.* **2020**, *11*, 318.
[216] D. O. Scanlon, G. W. Watson, *J. Phys. Chem. Lett.* **2010**, *1*, 2582.
[217] C. Li, J. He, Y. Xiao, Y. Li, J. J. Delaunay, *Energy Environ. Sci.* **2020**, *13*, 3269.
[218] J. Herion, E. A. Niekisch, G. Scharl, *Sol. Energy Mater.* **1980**, *4*, 101.
[219] A. Mittiga, E. Salza, F. Sarto, M. Tucci, R. Vasanthi, *Appl. Phys. Lett.* **2006**, *88*, 163502.
[220] T. Minami, Y. Nishi, T. Miyata, *Appl. Phys. Express* **2016**, *9*, 052301.
[221] T. Minami, Y. Nishi, T. Miyata, *Appl. Phys. Express* **2015**, *8*, 022301.
[222] R. N. Briskman, *Sol. Energy Mater. Sol. Cells* **1992**, *27*, 361.
[223] S. S. Jeong, A. Mittiga, E. Salza, A. Masci, S. Passerini, *Electrochim. Acta* **2008**, *53*, 2226.
[224] G. C. Lee, Y. S. Jung, K. H. Kim, *Mol. Cryst. Liq. Cryst.* **2014**, *598*, 62.
[225] M. Patel, S.-H. Park, J. Kim, *Phys. Status Solidi* **2018**, *215*, 1800216.
[226] Y. Ievskaya, R. L. Z. Hoye, A. Sadhanala, K. P. Musselman, J. L. MacManus-Driscoll, *Sol. Energy Mater. Sol. Cells* **2015**, *135*, 43.
[227] N. Winkler, S. Edinger, J. Kaur, R. A. Wibowo, W. Kautek, T. Dimopoulos, *J. Mater. Sci.* **2018**, *53*, 12231.
[228] S. Thambidurai, P. Gowthaman, M. Venkatachalam, S. Suresh, M. Kandasamy, *J. Alloys Compd.* **2021**, *852*, 156997.
[229] H. Behzad, F. E. Ghodsi, E. Peksu, H. Karaagac, *J. Alloys Compd.* **2018**, *744*, 470.
[230] S. Rühle, A. Y. Anderson, H.-N. Barad, B. Kupfer, Y. Bouhadana, E. Rosh-Hodesh, A. Zaban, *J. Phys. Chem. Lett.* **2012**, *3*, 3755.
[231] S. Chatterjee, S. K. Saha, A. J. Pal, *Sol. Energy Mater. Sol. Cells* **2016**, *147*, 17.
[232] A. Costas, C. Florica, N. Preda, N. Apostol, A. Kuncser, A. Nitescu, I. Enculescu, *Sci. Rep.* **2019**, *9*, 5553.
[233] W. Shockley, H. J. Queisser, *J. Appl. Phys.* **1961**, *32*, 510.
[234] R. P. Wijesundera, L. K. A. D. D. S. Gunawardhana, W. Siripala, *Sol. Energy Mater. Sol. Cells* **2016**, *157*, 881.
[235] N. Yantara, N. Mathews, K. B. Jinesh, H. K. Mulmudi, S. G. Mhaisalkar, *Electrochim. Acta* **2012**, *85*, 486.
[236] P. Ghamgosar, F. Rigoni, S. You, I. Dobryden, M. G. Kohan, A. L. Pellegrino, I. Concina, N. Almqvist, G. Malandrino, A. Vomiero, *Nano Energy* **2018**, *51*, 308.

[237] S. S. Wilson, J. P. Bosco, Y. Tolstova, D. O. Scanlon, G. W. Watson, H. A. Atwater, *Energy Environ. Sci.* **2014**, *7*, 3606.
[238] A. Živković, A. Roldan, N. H. de Leeuw, *Phys. Rev. B* **2019**, *99*, 035154.
[239] B. Kupfer, K. Majhi, D. A. Keller, Y. Bouhadana, S. Rühle, H. N. Barad, A. Y. Anderson, A. Zaban, *Adv. Energy Mater.* **2015**, *5*, 1401007.
[240] M. Gilzad Kohan, G. Solomon, S. You, K. Yusupov, I. Concina, A. Vomiero, *Nano Select* **2021**, *2*, 967.
[241] T. T. Nguyen, M. Patel, J. Kim, *Sol. Energy Mater. Sol. Cells* **2020**, *217*, 110708.
[242] D. B. Patel, K. R. Chauhan, *J. Alloys Compd.* **2020**, *842*, 155594.
[243] L. Tian, J. Föhlinger, Z. Zhang, P. B. Pati, J. Lin, T. Kubart, Y. Hua, J. Sun, L. Kloo, G. Boschloo, L. Hammarström, H. Tian, *Chem. Commun.* **2018**, *54*, 3739.
[244] H. Tian, *Sustainable Energy Fuels* **2019**, *3*, 888.
[245] M. Ghini, N. Curreli, A. Camellini, M. Wang, A. Asaithambi, I. Kriegel, *Nanoscale* **2021**, *13*, 8773.
[246] G. M. Carroll, A. M. Schimpf, E. Y. Tsui, D. R. Gamelin, *J. Am. Chem. Soc.* **2015**, *137*, 11163.
[247] G. Wang, L. Zhang, J. Zhang, *Chem. Soc. Rev.* **2012**, *41*, 797.
[248] C. K. Brozek, K. H. Hartstein, D. R. Gamelin, *J. Am. Chem. Soc.* **2016**, *138*, 10605.
[249] I. Kriegel, M. Ghini, S. Bellani, K. Zhang, A. W. Jansons, B. M. Crockett, K. M. Koskela, E. S. Barnard, E. Penzo, J. E. Hutchison, J. A. Robinson, L. Manna, N. J. Borys, P. J. Schuck, *J. Phys. Chem. C* **2020**, *124*, 8000.
[250] C. J. Dahlman, Y. Tan, M. A. Marcus, D. J. Milliron, *J. Am. Chem. Soc.* **2015**, *137*, 9160.
[251] P. R. Bueno, *J. Power Sources* **2019**, *414*, 420.
[252] Y. Xu, Z. Lin, X. Zhong, X. Huang, N. O. Weiss, Y. Huang, X. Duan, *Nat. Commun.* **2014**, *5*, 4554.
[253] D. Sheberla, J. C. Bachman, J. S. Elias, C.-J. Sun, Y. Shao-Horn, M. Dincă, *Nat. Mater.* **2017**, *16*, 220.
[254] Q. Zeng, Y. Lai, L. Jiang, F. Liu, X. Hao, L. Wang, M. A. Green, *Adv. Energy Mater.* **2020**, *10*, 1903930.
[255] M. Ghini, E. S. Yanev, C. Kastl, K. Zhang, A. W. Jansons, B. M. Crockett, K. M. Koskela, E. S. Barnard, E. Penzo, J. E. Hutchison, J. A. Robinson, L. Manna, N. J. Borys, P. J. Schuck, I. Kriegel, *Adv. Photonics Res.* **2021**, *2*, 2000151.
[256] W. Guo, L. Wu, Z. Chen, G. Boschloo, A. Hagfeldt, T. Ma, *J. Photochem. Photobiol., A* **2011**, *219*, 180.
[257] V. Postica, M. Hoppe, J. Gröttrup, P. Hayes, V. Röbisch, D. Smazna, R. Adelung, B. Viana, P. Aschehoug, T. Pauporté, O. Lupan, *Solid State Sci.* **2017**, *71*, 75.
[258] U. Banin, N. Waiskopf, L. Hammarström, G. Boschloo, M. Freitag, E. M. J. Johansson, J. Sá, H. Tian, M. B. Johnston, L. M. Herz, R. L. Milot, M. G. Kanatzidis, W. Ke, I. Spanopoulos, K. L. Kohlstedt, G. C. Schatz, N. Lewis, T. Meyer, A. J. Nozik, M. C. Beard, F. Armstrong, C. F. Megarity, C. A. Schmuttenmaer, V. S. Batista, G. W. Brudvig, *Nanotechnology* **2020**, *32*, 042003.
[259] B. O'Regan, M. Grätzel, *Nature* **1991**, *353*, 737.
[260] M. Freitag, J. Teuscher, Y. Saygili, X. Zhang, F. Giordano, P. Liska, J. Hua, S. M. Zakeeruddin, J.-E. Moser, M. Grätzel, A. Hagfeldt, *Nat. Photonics* **2017**, *11*, 372.
[261] Y. Cao, Y. Liu, S. M. Zakeeruddin, A. Hagfeldt, M. Grätzel, *Joule* **2018**, *2*, 1108.
[262] M. Green, E. Dunlop, J. Hohl-Ebinger, M. Yoshita, N. Kopidakis, X. Hao, *Prog. Photovoltaics Res. Appl.* **2021**, *29*, 3.
[263] C. Cavallo, F. Di Pascasio, A. Latini, M. Bonomo, D. Dini, *J. Nanomater.* **2017**, *2017*, 5323164.
[264] C. Aumaitre, D. Joly, D. Aldakov, R. Demadrille, in *Metal Oxides* (Ed: M. B. T. Lira-Cantu), Elsevier, New York **2018**, pp. 85–115.
[265] J. Wu, Z. Lan, J. Lin, M. Huang, Y. Huang, L. Fan, G. Luo, *Chem. Rev.* **2015**, *115*, 2136.
[266] A. Carella, F. Borbone, R. Centore, *Front. Chem.* **2018**, *6*, 481.
[267] M.-E. Yeoh, K.-Y. Chan, *Int. J. Energy Res.* **2017**, *41*, 2446.
[268] B. C. O'Regan, J. R. Durrant, P. M. Sommeling, N. J. Bakker, *J. Phys. Chem. C* **2007**, *111*, 14001.
[269] T. Peng, K. Fan, D. Zhao, J. Chen, *J. Phys. Chem. C* **2010**, *114*, 22346.
[270] T. W. Hamann, O. K. Farha, J. T. Hupp, *J. Phys. Chem. C* **2008**, *112*, 19756.
[271] R. Ruess, J. Horn, A. Ringleb, D. Schlettwein, *J. Phys. Chem. C* **2019**, *123*, 22074.
[272] R. Vittal, K.-C. Ho, *Renewable Sustainable Energy Rev.* **2017**, *70*, 920.
[273] T. Yoshida, J. Zhang, D. Komatsu, S. Sawatani, H. Minoura, T. Pauporté, D. Lincot, T. Oekermann, D. Schlettwein, H. Tada, D. Wöhrle, K. Funabiki, M. Matsui, H. Miura, H. Yanagi, *Adv. Funct. Mater.* **2009**, *19*, 17.
[274] J. A. Anta, E. Guillén, R. Tena-Zaera, *J. Phys. Chem. C* **2012**, *116*, 11413.
[275] C. Klingshirn, J. Fallert, H. Zhou, J. Sartor, C. Thiele, F. Maier-Flaig, D. Schneider, H. Kalt, *Phys. Status Solidi* **2010**, *247*, 1424.
[276] Z. Qin, Y. Huang, Q. Liao, Z. Zhang, X. Zhang, Y. Zhang, *Mater. Lett.* **2012**, *70*, 177.
[277] K. Prabakar, M. Son, W.-Y. Kim, H. Kim, *Mater. Chem. Phys.* **2011**, *125*, 12.
[278] C. Justin Raj, S. N. Karthick, K. V Hemalatha, M.-K. Son, H.-J. Kim, K. Prabakar, *J. Sol-Gel Sci. Technol.* **2012**, *62*, 453.
[279] X. Guo, H. Dong, G. Niu, Y. Qiu, L. Wang, *RSC Adv.* **2014**, *4*, 21294.
[280] C. J. Raj, K. Prabakar, S. N. Karthick, K. V Hemalatha, M.-K. Son, H.-J. Kim, *J. Phys. Chem. C* **2013**, *117*, 2600.
[281] A. Ringleb, R. Ruess, N. Hofeditz, W. Heimbrodt, T. Yoshida, D. Schlettwein, *Phys. Chem. Chem. Phys.* **2021**, *23*, 8393.
[282] S. Yun, J. Lee, J. Chung, S. Lim, *J. Phys. Chem. Solids* **2010**, *71*, 1724.
[283] S. Zhu, X. Tian, L. Shan, Z. Ding, Z. Kan, X. Xu, Z. Zhou, L. Wang, *Ceram. Int.* **2013**, *39*, 9637.
[284] S. R. Bhattacharyya, Z. Mallick, R. N. Gayen, *J. Electron. Mater.* **2020**, *49*, 3860.
[285] Q. Wali, A. Fakharuddin, R. Jose, *J. Power Sources* **2015**, *293*, 1039.
[286] A. Pallikkara, K. Ramakrishnan, *Int. J. Energy Res.* **2021**, *45*, 1425.
[287] D. Hwang, J.-S. Jin, H. Lee, H.-J. Kim, H. Chung, D. Y. Kim, S.-Y. Jang, D. Kim, *Sci. Rep.* **2014**, *4*, 7353.
[288] S. S. Shin, J. S. Kim, J. H. Suk, K. D. Lee, D. W. Kim, J. H. Park, I. S. Cho, K. S. Hong, J. Y. Kim, *ACS Nano* **2013**, *7*, 1027.
[289] C. J. Wood, G. H. Summers, C. A. Clark, N. Kaeffer, M. Braeutigam, L. R. Carbone, L. D'Amario, K. Fan, Y. Farré, S. Narbey, F. Oswald, L. A. Stevens, C. D. J. Parmenter, M. W. Fay, A. La Torre, C. E. Snape, B. Dietzek, D. Dini, L. Hammarström, Y. Pellegrin, F. Odobel, L. Sun, V. Artero, E. A. Gibson, *Phys. Chem. Chem. Phys.* **2016**, *18*, 10727.
[290] L. Wei, L. Jiang, S. Yuan, X. Ren, Y. Zhao, Z. Wang, M. Zhang, L. Shi, D. Li, *Electrochim. Acta* **2016**, *188*, 309.
[291] G. Natu, P. Hasin, Z. Huang, Z. Ji, M. He, Y. Wu, *ACS Appl. Mater. Interfaces* **2012**, *4*, 5922.
[292] C. J. Flynn, S. M. McCullough, E. Oh, L. Li, C. C. Mercado, B. H. Farnum, W. Li, C. L. Donley, W. You, A. J. Nozik, J. R. McBride, T. J. Meyer, Y. Kanai, J. F. Cahoon, *ACS Appl. Mater. Interfaces* **2016**, *8*, 4754.
[293] V. Nikolaou, A. Charisiadis, G. Charalambidis, A. G. Coutsolelos, F. Odobel, *J. Mater. Chem. A* **2017**, *5*, 21077.
[294] L. D'Amario, J. Föhlinger, G. Boschloo, L. Hammarström, *Chem. Sci.* **2018**, *9*, 223.
[295] O. Langmar, C. R. Ganivet, G. de la Torre, T. Torres, R. D. Costa, D. M. Guldi, *Nanoscale* **2016**, *8*, 17963.
[296] A. Renaud, L. Cario, P. Deniard, E. Gautron, X. Rocquefelte, Y. Pellegrin, E. Blart, F. Odobel, S. Jobic, *J. Phys. Chem. C* **2014**, *118*, 54.
[297] S. Powar, D. Xiong, T. Daeneke, M. T. Ma, A. Gupta, G. Lee, S. Makuta, Y. Tachibana, W. Chen, L. Spiccia, Y.-B. Cheng, G. Götz, P. Bäuerle, U. Bach, *J. Phys. Chem. C* **2014**, *118*, 16375.

[298] J. Bai, X. Xu, L. Xu, J. Cui, D. Huang, W. Chen, Y. Cheng, Y. Shen, M. Wang, *ChemSusChem* **2013**, *6*, 622.
[299] H. Yuan, W. Wang, D. Xu, Q. Xu, J. Xie, X. Chen, T. Zhang, C. Xiong, Y. He, Y. Zhang, Y. Liu, H. Shen, *Sol. Energy* **2018**, *165*, 233.
[300] L. M. Peter, *Philos. Trans. R. Soc., A* **2011**, *15*, 1.
[301] J. M. Kroon, N. J. Bakker, H. J. P. Smit, P. Liska, K. R. Thampi, P. Wang, S. M. Zakeeruddin, M. Grätzel, A. Hinsch, S. Hore, U. Würfel, R. Sastrawan, J. R. Durrant, E. Palomares, H. Pettersson, T. Gruszecki, J. Walter, K. Skupien, G. E. Tulloch, *Prog. Photovoltaics Res. Appl.* **2007**, *15*, 1.
[302] Y. Wang, A. B. Djurišić, W. Chen, F. Liu, R. Cheng, S. Ping Feng, A. M. C. Ng, Z. He, *J. Phys. Energy* **2020**, *3*, 012004.
[303] P. Topolovsek, F. Lamberti, T. Gatti, A. Cito, J. M. Ball, E. Menna, C. Gadermaier, A. Petrozza, *J. Mater. Chem. A* **2017**, *5*, 11882.
[304] Y. Chen, Q. Meng, L. Zhang, C. Han, H. Gao, Y. Zhang, H. Yan, *J. Energy Chem.* **2019**, *35*, 144.
[305] C.-Q. Luo, F. C.-C. Ling, M. A. Rahman, M. Phillips, C. Ton-That, C. Liao, K. Shih, J. Lin, H. W. Tam, A. B. Djurišić, S.-P. Wang, *Appl. Surf. Sci.* **2019**, *483*, 1129.
[306] S. Phillips, W. Warmuth, *Fraunhofer ISE: Photovoltaics Report*, **2020**.
[307] "Best Research-Cell Efficiency Chart," (accessed: April 2021).
[308] T. Baikie, Y. Fang, J. M. Kadro, M. Schreyer, F. Wei, S. G. Mhaisalkar, M. Graetzel, T. J. White, *J. Mater. Chem. A* **2013**, *1*, 5628.
[309] *Solar Cells and Light Management: Materials, Strategies and Sustainability* (Eds: F. Enrichi, G. C. Righini), Elsevier, New York **2019**.
[310] K. Chan, M. Wright, N. Elumalai, A. Uddin, S. Pillai, *Adv. Opt. Mater.* **2017**, *5*, 1600698.
[311] F. Enrichi, A. Quandt, G. C. Righini, *Renewable Sustainable Energy Rev.* **2018**, *82*, 2433.
[312] Y. Wang, P. Shen, J. Liu, Y. Xue, Y. Wang, M. Yao, L. Shen, *Sol. RRL* **2019**, *3*, 1900181.
[313] H. Zhang, J. Toudert, *Sci. Technol. Adv. Mater.* **2018**, *19*, 411.
[314] Y. Shang, S. Hao, C. Yang, G. Chen, *Nanomaterials* **2015**, *5*, 1782.
[315] M. B. de la Mora, O. Amelines-Sarria, B. M. Monroy, C. D. Hernández-Pérez, J. E. Lugo, *Sol. Energy Mater. Sol. Cells* **2017**, *165*, 59.
[316] J. Day, S. Senthilarasu, T. K. Mallick, *Renewable Energy* **2019**, *132*, 186.
[317] T. Trupke, M. A. Green, P. Würfel, *J. Appl. Phys.* **2002**, *92*, 1668.
[318] T. Trupke, M. A. Green, P. Würfel, *J. Appl. Phys.* **2002**, *92*, 4117.
[319] X. Huang, S. Han, W. Huang, X. Liu, *Chem. Soc. Rev.* **2013**, *42*, 173.
[320] *Spectroscopic Properties of Rare Earths in Optical Materials* (Eds: G. Liu, B. Jacquier), Springer, Berlin **2006**.
[321] A. Gulzar, J. Xu, P. Yang, F. He, L. Xu, *Nanoscale* **2017**, *9*, 12248.
[322] B. Boulard, T. T. T. Van, A. Łukowiak, A. Bouajaj, R. R. Gonçalves, A. Chiappini, A. Chiasera, W. Blanc, A. Duran, S. Turrell, F. Prudenzano, F. Scotognella, R. Ramponi, M. Marciniak, G. C. Righini, M. Ferrari, *Photonic Glass-Ceramics: Consolidated Outcomes and Prospects*, Proc. SPIE 9364, Oxide-based Materials and Devices VI, March **2015**, 93640Z, https://doi.org/10.1117/12.2078263.
[323] G. Chen, C. Yang, P. N. Prasad, *Acc. Chem. Res.* **2013**, *46*, 1474.
[324] G. Gorni, J. J. Velázquez, J. Mosa, R. Balda, J. Fernández, A. Durán, Y. Castro, *Materials* **2018**, *11*, 212.
[325] F. Enrichi, C. Armellini, S. Belmokhtar, A. Bouajaj, A. Chiappini, M. Ferrari, A. Quandt, G. C. Righini, A. Vomiero, L. Zur, *J. Lumin.* **2018**, *193*, 44.
[326] F. Enrichi, E. Cattaruzza, T. Finotto, P. Riello, G. C. Righini, E. Trave, A. Vomiero, *Appl. Sci.* **2020**, *10*, 2184.
[327] H. Lin, D. Chen, Y. Yu, R. Zhang, Y. Wang, *Appl. Phys. Lett.* **2013**, *103*, 091902.
[328] H. Wang, S. Ye, T. Liu, S. Li, D. Wang, *J. Am. Ceram. Soc.* **2016**, *99*, 2376.
[329] F. Enrichi, C. Armellini, G. Battaglin, F. Belluomo, S. Belmokhtar, A. Bouajaj, E. Cattaruzza, M. Ferrari, F. Gonella, A. Lukowiak, M. Mardegan, S. Polizzi, E. Pontoglio, G. C. Righini, C. Sada, E. Trave, L. Zur, *Opt. Mater.* **2016**, *60*, 264.
[330] F. Enrichi, S. Belmokhtar, A. Benedetti, A. Bouajaj, E. Cattaruzza, F. Coccetti, E. Colusso, M. Ferrari, P. Ghamgosar, F. Gonella, M. Karlsson, A. Martucci, R. Ottini, P. Riello, G. C. Righini, E. Trave, A. Vomiero, S. You, L. Zur, *Opt. Mater.* **2018**, *84*, 668.
[331] Y. Ning, Z. Zhang, F. Teng, X. Fang, *Small* **2018**, *14*, 1703754.
[332] B. R. West, *Opt. Eng.* **2011**, *50*, 071107.
[333] Y. He, J. Liu, S. J. Sung, C. hung Chang, *Mater. Des.* **2021**, *201*, 109454.
[334] K.-T. Lee, J.-H. Park, S. J. Kwon, H.-K. Kwon, J. Kyhm, K.-W. Kwak, H. S. Jang, S. Y. Kim, J. S. Han, S.-H. Lee, D.-H. Shin, H. Ko, I.-K. Han, B.-K. Ju, S.-H. Kwon, D.-H. Ko, *Nano Lett.* **2015**, *15*, 2491.
[335] H. Chen, S.-M. Lee, A. Montenegro, D. Kang, B. Gai, H. Lim, C. Dutta, W. He, M. L. Lee, A. Benderskii, J. Yoon, *ACS Photonics* **2018**, *5*, 4289.
[336] G. Maduraiveeran, M. Sasidharan, W. Jin, *Prog. Mater. Sci.* **2019**, *106*, 100574.
[337] H. Agarwal, S. Venkat Kumar, S. Rajeshkumar, *Resour. Technol.* **2017**, *3*, 406.
[338] B. Yuliarto, N. L. W. Septiani, Y. V. Kaneti, M. Iqbal, G. Gumilar, M. Kim, J. Na, K. C.-W. Wu, Y. Yamauchi, *New J. Chem.* **2019**, *43*, 15846.
[339] A. V. Nikam, B. L. V. Prasad, A. A. Kulkarni, *CrystEngComm* **2018**, *20*, 5091.
[340] Y. Zhang, X. Xu, *ACS Omega* **2020**, *5*, 15344.
[341] V. Sharma, P. Kumar, P. Dev, G. Pilania, *J. Appl. Phys.* **2020**, *128*, 034902.
[342] R. Dong, Y. Dan, X. Li, J. Hu, *Comput. Mater. Sci.* **2021**, *188*, 110166.
[343] Y. Zhang, X. Xu, *Optik* **2020**, *217*, 164808.
[344] C. N. R. Rao, *J. Phys. Chem. Lett.* **2015**, *6*, 3303.
[345] A. Ruiz Puigdollers, P. Schlexer, S. Tosoni, G. Pacchioni, *ACS Catal.* **2017**, *7*, 6493.
[346] A. Jafari, K. Tahani, D. Dastan, S. Asgary, Z. Shi, X.-T. Yin, W.-D. Zhou, H. Garmestani, Ş. Ţălu, *Surf. Interfaces* **2020**, *18*, 100463.
[347] C. W. White, L. A. Boatner, P. S. Sklad, C. J. Mchargue, S. J. Pennycook, M. J. Aziz, G. C. Farlow, J. Rankin, *MRS Proc.* **1986**, *74*, 357.
[348] N. Teranishi, G. Fuse, M. Sugitani, *Sensors* **2018**, *18*, 2358.
[349] D. Chen, Y. Wang, *Nanoscale* **2013**, *5*, 4621.
[350] Z. Li, M. K. Joshi, J. Chen, Z. Zhang, Z. Li, X. Fang, *Adv. Funct. Mater.* **2020**, *30*, 2005291.
[351] A. Chen, Q. Su, H. Han, E. Enriquez, Q. Jia, *Adv. Mater.* **2019**, *31*, 1803241.
[352] B. M. Crockett, A. W. Jansons, K. M. Koskela, D. W. Johnson, J. E. Hutchison, *ACS Nano* **2017**, *11*, 7719.
[353] A. W. Jansons, K. M. Koskela, B. M. Crockett, J. E. Hutchison, *Chem. Mater.* **2017**, *29*, 8167.
[354] A. W. Jansons, L. K. Plummer, J. E. Hutchison, *Chem. Mater.* **2017**, *29*, 5415.
[355] E. L. Runnerstrom, A. Bergerud, A. Agrawal, R. W. Johns, C. J. Dahlman, A. Singh, S. M. Selbach, D. J. Milliron, *Nano Lett.* **2016**, *16*, 3390.
[356] J. Xiong, J. Di, J. Xia, W. Zhu, H. Li, *Adv. Funct. Mater.* **2018**, *28*, 1801983.
[357] M. S. Chavali, M. P. Nikolova, *SN Appl. Sci.* **2019**, *1*, 607.
[358] A. Bailini, F. Di Fonzo, M. Fusi, C. S. Casari, A. L. Bassi, V. Russo, A. Baserga, C. E. Bottani, *Appl. Surf. Sci.* **2007**, *253*, 8130.
[359] G. Tabacchi, E. Fois, D. Barreca, A. Gasparotto, *Phys. Status Solidi* **2014**, *211*, 251.
[360] P. Cop, E. Celik, K. Hess, Y. Moryson, P. Klement, M. T. Elm, B. M. Smarsly, ACS Appl, *Nano Mater.* **2020**, *3*, 10757.

[361] S. H. Salman, A. A. Shihab, A.-H. Kh, Elttayef, *Energy Procedia* **2019**, *157*, 283.
[362] W. Stepniowski, W. Misiolek, *Nanomaterials* **2018**, *8*, 379.
[363] *Solution Processed Metal Oxide Thin Films for Electronic Applications* (Eds: Z. Cui, G. Korotcenkov) Elsevier, New York **2020**.
[364] P. Kumbhakar, C. Chowde Gowda, P. L. Mahapatra, M. Mukherjee, K. D. Malviya, M. Chaker, A. Chandra, B. Lahiri, P. M. Ajayan, D. Jariwala, A. Singh, C. S. Tiwary, *Mater. Today* **2021**, https://doi.org/10.1016/j.mattod.2020.11.023.
[365] T. Yang, T. T. Song, M. Callsen, J. Zhou, J. W. Chai, Y. P. Feng, S. J. Wang, M. Yang, *Adv. Mater. Interfaces* **2019**, *6*, 1801160.

Teresa Gatti holds a master degree in Chemistry from the University of Bologna, Italy (2008) and a Ph.D. in Materials Engineering from Politecnico di Milano, Italy (2014). After postdoctoral activities at the Department of Chemical Sciences of the University of Padova (Italy), since 2019 she is a Group Leader at the Center for Materials Research of the Justus Liebig University Giessen (Germany). Her research interests cover the production, processing and application in optoelectronic devices of different emerging semiconducting materials, with special attention to species based on non-critical elements and featuring low-environmental impact.

Francesco Lamberti obtained his Ph.D. degree in Material Sciences and Engineering from the University of Padova in 2011. After studying electrochemical biosensors on optically transparent electrodes, he moved to the Italian Institute of Technology (IIT) in Milano, working in the group of Dr. Annamaria Petrozza on the development of perovskite solar cells. Currently, he holds a scientist position at the University of Padova focusing on the thin-film processing for emerging photovoltaics exploiting ultrasonic spraying system.

Silvia Gross is currently full professor of Inorganic Chemistry at the University of Padova. She is also a TUM visiting professor at the Technische Universität München and a DFG Mercator Fellow at the Karlsruher Institut für Technologie. She holds also a position as Project Technical Advisor of the European Cluster on Catalysis for the European Commission. Her current research activity is mainly focused on the synthesis and characterization of organically modified transition metal oxoclusters, and green synthesis of crystalline metal oxides by wet chemistry and colloidal routes, mainly miniemulsions and solvo/hydrothermal synthesis at low or room temperature.